NASA TECHNICAL NOTE

NASA TN D-2927

NASA TN D-2927

A TRANSONIC INVESTIGATION OF BASE PRESSURES ASSOCIATED WITH SHALLOW THREE-DIMENSIONAL REARWARD-FACING STEPS

by Thomas C. Kelly

Langley Research Center
Langley Station, Hampton, Va.

NATIONAL AERONAUTICS AND SPACE ADMINISTRATION • WASHINGTON, D. C. • AUGUST 1965

A TRANSONIC INVESTIGATION OF BASE PRESSURES ASSOCIATED WITH SHALLOW THREE-DIMENSIONAL REARWARD-FACING STEPS

By Thomas C. Kelly

Langley Research Center
Langley Station, Hampton, Va.

NATIONAL AERONAUTICS AND SPACE ADMINISTRATION

For sale by the Clearinghouse for Federal Scientific and Technical Information
Springfield, Virginia 22151 – Price $2.00

A TRANSONIC INVESTIGATION OF BASE PRESSURES ASSOCIATED WITH SHALLOW THREE-DIMENSIONAL REARWARD-FACING STEPS

By Thomas C. Kelly
Langley Research Center

SUMMARY

Results have been obtained which show effects on rearward-facing-step base pressures of variations in step height for simulated launch-vehicle configurations where the steps were located both close to and considerably downstream of the nose-cone—cylinder junctures. The investigation was conducted over a Mach number range from 0.40 to 1.20 at an angle of attack of 0°.

The results indicated that, for a typical launch-vehicle model used to simulate the case where the step was located at a considerable distance downstream of the nose-cone—cylinder juncture, step base pressure coefficients were found to be relatively insensitive to variations in Reynolds number. Slight effects of Reynolds number were noted, however, both in the cylinder surface pressure coefficients preceding a step and in the step base pressure coefficients for a configuration simulating the case where the step was located close to the nose-cone—cylinder juncture.

For both 15° and 30° nose-cone—cylinder models, locating the step within the influence of the pressure fields associated with the nose-cone—cylinder junctures resulted in step base pressure variations with Mach number which were considerably more abrupt and about five times more severe than those for the case where the step was located several body diameters downstream of the juncture.

Generally, the variation of step base pressure coefficient with variation in step height was relatively gradual for all configurations.

Significant effects of transition-strip location were noted for a 30° nose-cone—cylinder configuration which served to emphasize the need for careful application of such strips in order to obtain accurate measurements of the local distributed loads for scaled launch-vehicle models.

INTRODUCTION

The use of shallow, rearward-facing steps is occasionally required in the development of launch vehicles. Inasmuch as the steps generally occur over regions of the vehicle where internal compartments must be vented to the

external stream, they are often considered for use as vents, and it therefore becomes a matter of practical importance to determine the base pressures associated with these steps.

Considerable theoretical and experimental effort has been directed to the problem of determining base pressures and the various factors influencing base pressures. (See, for example, refs. 1 to 4.) In the application of these results to the problem of step base pressures, the investigations pertaining to sting-support interference effects are most important since the combination of a model afterbody and a support sting forms a rearward-facing step. Two factors, however, often preclude a direct application of the sting-interference results. First, for most sting-interference investigations, the ratios of sting diameter to base diameter are significantly less than 1.0 and therefore correspond to unusually large steps. Secondly, the model base (or step) is generally not located close to variations in local geometry such as nose-cone—cylinder or flare-cylinder junctures, whereas this is often the case on launch vehicles. Consequently, on launch vehicles, step base pressures may be considerably influenced by nonuniform flow and viscous effects.

The present investigation was undertaken to determine the effects on step base pressures of variations in step height for configurations where the steps were located both within and outside of the influence of nose-cone—cylinder junctures. To simulate the step located within the influence of the juncture, nose-cone—cylinder models were employed which had cylinder fineness ratios (upstream of the step) of 1.0 and 0.5. Nose-cone half-angles of 15° and 30° were used with these configurations. The case of the step removed from juncture influence was simulated by using an existing launch-vehicle model. For this configuration, the cylinder fineness ratio upstream of the step was 7.0.

The investigation was conducted in the Langley 8-foot transonic pressure tunnel over a Mach number range from 0.40 to 1.20 at an angle of attack of 0°. The Reynolds number per foot was generally held constant at 4.0×10^6; however, for selected configurations additional tests were conducted at a Reynolds number per foot of 2.0×10^6.

SYMBOLS

Coefficients and symbols used in this paper are defined as follows:

C_p local pressure coefficient, $\frac{p_l - p_\infty}{q_\infty}$

$C_{p,b}$ step base pressure coefficient, $\frac{p_b - p_\infty}{q_\infty}$

d diameter of body following step, in.

D diameter of body ahead of step, in.

l longitudinal distance from nose-cone—cylinder juncture to step, in.

M Mach number

p_b static pressure at step base, lb/sq ft

p_l local static pressure, lb/sq ft

p_∞ free-stream static pressure, lb/sq ft

q_∞ free-stream dynamic pressure, lb/sq ft

R_{ft} Reynolds number per foot

R_l Reynolds number based on model length

x longitudinal distance, measured from nose-cone—cylinder juncture, in.

δ_N nose-cone half-angle, deg

ϕ base orifice orientation angle, measured clockwise from the vertical as viewed from the rear, deg

Subscript:

sonic corresponding to a local Mach number of 1.0

APPARATUS AND TESTS

Models

Details and design dimensions of the model configurations employed in the present investigation are shown in figure 1. For all configurations, the ratio of the diameter following the step to the diameter ahead of the step was varied by using wooden sleeves which were clamped about the usual model-support sting and which extended rearward from the step base. The fineness ratio of the sleeve following the step varied slightly with configuration; however, based upon the results of reference 3, the sleeves were always of sufficient length to eliminate any interference effects on base pressures caused by the sting flare.

The configuration illustrated in figure 1(a) consisted of a typical launch-vehicle model in combination with several sting sleeves. These models were utilized to represent the case where the step is located at a considerable distance downstream of a juncture. For these configurations, six orifices were located on the model base at roll angles (measured clockwise from the vertical as viewed from the rear) of 0°, 45°, 90°, 135°, 180°, and 270°. (See fig. 1(a).)

The nose-cone—cylinder configurations described in the following section were designed to simulate cases where the steps were located close to, and slightly downstream of, a nose-cone—cylinder juncture and were therefore immersed in the nonuniform flow field associated with the nose-cone—cylinder juncture.

Model configurations shown in figure 1(b) utilized a 15° half-angle pointed nose cone in combination with a cylinder having a fineness ratio of 1.0 and several of the wooden sleeves. For these configurations four pressure orifices were installed in the step base at 90° circumferential intervals. In addition, a single orifice row was installed along the surface of the cylinder preceding the step at the locations given in the figure.

The configurations shown in figure 1(c) consisted of a 30° half-angle pointed nose cone in combination with a cylinder having a fineness ratio of 1.0 and selected wooden sleeves. Orifice locations along the cylinder surface and at the step base were identical to those for the previously described 15° half-angle nose-cone configurations which are tabulated in figure 1(b).

In addition to the configurations previously noted, the 15° and 30° half-angle nose cones were tested in combination with a cylinder having a fineness ratio of 0.5 and the wooden sleeve which resulted in the shallowest step ($d/D = 0.952$). Four step base orifices were installed at 90° circumferential intervals, and orifices were installed on the cylinder surface ahead of the step at the locations indicated in figure 1(d).

A summary of the configurations investigated is presented as table I.

Tests and Procedure

The investigation was conducted through a Mach number range extending from 0.40 to 1.20 at an angle of attack of 0°. All configurations were investigated at a Reynolds number per foot of 4.0×10^6 and at Mach numbers from 0.60 to 1.20. Because of tunnel limitations, the Reynolds number per foot at a Mach number of 0.40 was limited to 3.6×10^6. In addition, selected configurations were investigated at a Reynolds number per foot of 2.0×10^6.

In an effort to minimize any effects of wind-tunnel-wall disturbances or free-stream local Mach number variations, all configurations were investigated with the step at the same location relative to the tunnel.

Transition strips, composed of No. 60 carborundum grains set in a plastic adhesive, were applied to all configurations to insure turbulent flow. For the typical launch-vehicle model, the strips were added immediately behind the nose-cone—cylinder juncture. For the cone-cylinder models, the strips were positioned $1\frac{1}{2}$ inches rearward of the nose-cone apex measured along the slant surface. For selected cone-cylinder models (configurations 125, 224, 225, and 234), additional tests were made with a second transition strip located with the leading edge at the nose-cone—cylinder juncture.

Local and step base pressures on the models were measured by means of a multiple-tube manometer board and were photographically recorded.

Accuracy

A consideration of factors affecting the accuracy of the results indicates that for the investigations conducted at the higher Reynolds numbers the measured pressure coefficients are generally accurate within the following limits:

Mach number	C_p
0.4	±0.010
.8	±.008
1.2	±.006

For the typical launch-vehicle configurations, the step base pressure data are subject to error resulting from boundary-reflected disturbances which occur at Mach numbers from 1.03 to approximately 1.16. No attempt has been made to estimate the magnitude of the errors or to adjust the measured results for boundary interference. Figure 2 gives the present results (configuration 111) and those of reference 3 for a similar configuration. In both sets of data, sizable effects of boundary disturbances are indicated by the erratic variations in step base pressure coefficient at low supersonic speeds. It should be noted that the fairing of the present results at Mach numbers between 1.025 and 1.10 (shown dashed) is based upon the results obtained at a Mach number of 1.05 for configuration 113 (see table II(d)).

Estimates have indicated that, because of the foreshortened length to the step, results for the cone-cylinder configurations of the present investigation are free of boundary-interference effects for all Mach numbers at which data were recorded.

It should also be noted here that in some instances (notably, the results for the 30° cone-cylinder configurations at Mach numbers from about 0.60 to 0.90), wide variations exist between the individual step base pressure coefficients for a given configuration and the corresponding local pressure coefficients ahead of the step for successive runs of similar configurations. These variations and their causes are discussed in a following section.

PRESENTATION OF RESULTS

Results of the investigation are presented in the form of pressure coefficients (based on free-stream dynamic pressure) in tables II to IV. Inasmuch as the same model configuration was, in some cases, investigated at various Reynolds numbers or with differing transition strips, care should be exercised in selecting results from the tables for a particular configuration. The following is a list of figures in which selected results from these tables have been plotted for comparison:

DISCUSSION

Launch-Vehicle Model

Effect of Reynolds number.- The effects of a variation in Reynolds number on the average step base pressure coefficients for the typical launch-vehicle model are illustrated in figure 3. For both step heights presented, the results show essentially no effect at subsonic speeds of varying the Reynolds number per foot from 2.0×10^6 to 4.0×10^6 (or, from 6.93×10^6 to 13.86×10^6 based on body length). At Mach numbers from about 0.95 to 1.20, slight differences between the results obtained at the two Reynolds numbers are noted; however, no significance is attached to the variations in that they appear somewhat random in nature and are of a magnitude generally exceeded by the possible error of measurement. Furthermore, the results of reference 1 indicate that little effect of Reynolds number is to be expected at supersonic speeds for the condition where the boundary layer is turbulent ahead of the base for relatively high fineness ratio configurations.

Effect of step height.- The effects of a variation in base step height for the typical launch-vehicle model are shown for several Mach numbers in figure 4. These results are for a Reynolds number per foot of 4.0×10^6 $(R_l = 13.86 \times 10^6)$ and are compared with the sting interference results for the cylindrical-afterbody model of reference 3 $(R_l = 8.0 \times 10^6)$. The flagged

symbols shown in figure 4 at a diameter ratio d/D of 0.44 represent results obtained from earlier unpublished tests and are for the sting alone as shown in the top sketch of figure 1(a). In general, excellent agreement is noted except for the Mach number range from 1.00 to 1.10. The discrepancy at a Mach number of 1.00 may be a result of small differences in Mach number between the two investigations since sizable changes in step base pressure occur with slight variations in Mach number near a Mach number of 1. At the higher Mach numbers (M = 1.025 and M = 1.10), the results for both investigations are undoubtedly affected by boundary-interference effects. (See fig. 2.)

For most Mach numbers, the variation of step base pressure coefficient with step height is seen to be relatively gradual. Increases in the step diameter ratio (decreasing step height) are accompanied by an increase in the negative value of the step base pressure coefficient to some peak value which occurs at diameter ratios ranging from 0.71 at a Mach number of 0.60 to 0.87 at a Mach number of 1.20. Thereafter, the base pressure coefficients tend toward a value of 0, which would be realized at a diameter ratio of 1.0. The greatest variations in step base pressure coefficient with diameter ratio occur at Mach numbers near 0.95, where the base pressure coefficients are close to those corresponding to a local Mach number of unity $\left(C_{p,sonic} = -0.088\right)$.

Nose-Cone—Cylinder Models

Effect of transition-strip arrangement.- As a result of the unusual variations with Mach number noted in the local pressures both ahead of and at the step base for the 30° half-angle conical-nose configurations, brief tests were conducted to determine the effects of transition-strip arrangement. Two transition-strip arrangements were employed during this part of the investigation. The first consisted of a single band of transition particles located $1\frac{1}{2}$ inches rearward of the nose-cone apex measured along the slanted surface of the cone. The second arrangement employed an additional transition strip located with the leading edge at the nose-cone—cylinder juncture. Results for the 30° and 15° nose-cone configurations are presented in figures 5 and 6, respectively. Selected schlieren photographs are given in figure 7.

Examination of the results for the 30° nose-cone configurations (fig. 5) indicates that with the single strip located on the slanted surface of the cone, flow separation occurs immediately behind the nose-cone—cylinder juncture at Mach numbers from 0.40 to 0.90. It should also be noted that at a Mach number of 0.90, two types of flow (attached or separated rearward of the nose-cone—cylinder juncture) could be obtained depending upon the direction of tunnel airspeed approach to that Mach number during the investigation. Because of the flow separation, it was conjectured that the highly favorable pressure gradient over the nose cone resulted in a boundary layer too stable for the single transition strip to be effective; thus, the boundary layer was probably laminar at the cone-cylinder juncture.

The addition of a second transition strip located at the juncture on the 30° nose-cone configurations produced significant changes in the flow at all Mach numbers below 0.95 (fig. 5). The flow condition rearward of the juncture

was found to be extremely sensitive to the condition of the transition strip at the juncture. For the case illustrated by the schlieren photograph of figure 7(c) ($M = 0.90$, lower photograph) transition strips were located both on the slanted surface of the cone and at the juncture. Inspection of the juncture transition strip following the test indicated a relative scarcity of particles on the lower surface; this condition apparently caused the unsymmetrical separation noted in the figure. Unpublished results from more recent investigations of relatively high-angle nose-cone configurations indicate that the angle of attack also has a significant effect on unsymmetrical flow separation at the nose-cone—cylinder juncture. The foregoing results indicate that careful attention to the application of boundary-layer transition is required in order to obtain accurate measurements of the local distributed loads for scaled launch-vehicle models.

Results showing the effects of transition-strip arrangement for the 15° nose-cone configurations are given in figure 6. In general, slight effects are noted throughout the Mach number range except for the orifices near the juncture that are influenced by the presence of the transition strip itself.

All results presented hereafter for the 15° nose-cone configurations are for the case where a single transition strip located on the slanted surface of the nose cone was employed. Results for the 30° nose-cone configuration, however, are for the double transition-strip arrangement.

Effect of Reynolds number.- The effect of varying Reynolds number per foot from 2.0×10^6 to 4.0×10^6 is given in figure 8 for the 15° nose-cone configuration having a cylinder fineness ratio of 1.0 and a step-to-base-diameter ratio of 0.952. The surface pressure coefficients on the cylinder preceding the step and the step base pressure coefficients (flagged data points) are both included. The results indicate only a slight effect with increasing Reynolds number being accompanied by a slight decrease in the negative values of both the cylinder surface and the step base pressure coefficients. The differences between the curves for the two Reynolds numbers are generally well within the total possible error of measurement; for example, at a Mach number of 0.80 a total error of 0.024 in pressure coefficient could conceivably occur. The consistency of the variations, however, suggests that a Reynolds number effect does exist and, further, an examination of the results given in reference 1 shows that a similar Reynolds number effect occurs for the bodies with a lower fineness ratio and turbulent boundary-layer flow. (See fig. 14(a) of ref. 1.) The present results indicate that the slight variations in the step base pressures with Reynolds number are associated with variations in the flow upstream of the base rather than in any change in the flow condition at the base itself.

Effect of step height.- Effects of a variation in step diameter ratio are given in figure 9 for the 15° nose-cone configurations with a cylinder fineness ratio of 1.0. Local pressure coefficients on the cylinder ahead of the step and step base pressure coefficients (flagged data points) are given for step diameter ratios from 0.832 to 0.952. Included for comparison are the cylinder surface pressure coefficients for a configuration having no step ($d/D = 1.0$).

These results show that at Mach numbers of 0.90 and less, only slight effects of step height (d/D ratio) occur in the step base pressure coefficients. The presence of the step, however, has a noticeable influence on the cylinder surface pressures ahead of the step. Increasing step height, that is, decreasing d/D ratio, causes the pressure coefficients upstream of the step to increase negatively at Mach numbers from 0.40 to 0.90. This effect is particularly evident in a comparison of results for the case of no step (d/D = 1.0) with those for the shallowest step (d/D = 0.952). At free-stream Mach numbers higher than 0.90, the local flow over the cylinder ahead of the step is completely supersonic and, as a result, little or no effect of the step is indicated in the cylinder surface pressure coefficients. However, sizable effects of step height may be noted in the step base pressure coefficients at a Mach number of 0.95, increases in step height being accompanied by decreases in the negative values of the step base pressure coefficients. These effects of step height decrease with increases in Mach number up to a Mach number of 1.20.

Effect of step location.- The effects of step location relative to a nose-cone—cylinder juncture are given for a step diameter ratio of 0.952 in figure 10. Results are presented for the 15° and 30° nose-cone configurations having cylinder fineness ratios of 0.5 and 1.0 at a Reynolds number per foot of 4.0×10^6. Also shown for comparison are results for the case of no step, designated in figure 10 as $l/D = \infty$.

As would be expected, the step base pressure coefficients are greatly affected by the local flow conditions on the cylinder in the vicinity of the step. These local effects are most noticeably illustrated for both nose-cone angles in the results presented in figure 10 for Mach numbers from 0.95 to 1.20. The strong dependence of the step base pressures on the cylinder surface pressures requires that, for cases where the step base is considered for use in vehicle venting, careful attention be directed to the variation of the step base pressure coefficient with Mach number. In particular, the formation and rearward movement of the normal deceleration shock wave associated with the expansion at the nose-cone—cylinder juncture can cause severe fluctuations in the pressures at the step base at high subsonic speeds. These effects are illustrated in figure 11 where the average step base pressure coefficients are plotted as a function of Mach number for the 15° and 30° cone-cylinder configurations having cylinder fineness ratios of 1.0 and 0.5. Also included for comparison are the base pressure coefficients for the typical launch-vehicle model and the variation with Mach number of $C_{p,sonic}$, the pressure coefficient corresponding to a local Mach number of 1.0. The step diameter ratio for all configurations is 0.952.

For the cone-cylinder configurations, where the step base falls within the influence of the nose-cone—cylinder juncture, several effects are noted. First, the subsonic level of the base pressure coefficient is increased negatively as the cylinder fineness ratio is decreased. This results from moving the step upstream into the low pressure region associated with the nose-cone—cylinder juncture. Secondly, the sudden negative increase in the step base pressure coefficients with increasing Mach number is generally preceded by an abrupt positive increase as a result of the rearward movement over the step location of the previously mentioned deceleration wave. As would be expected,

the initial positive increase in step base pressure coefficient occurs at lower free-stream Mach numbers as the distance from the juncture to the step is decreased. (See fig. 11.) It is also of interest to note that when the step is located in the pressure field of the nose-cone—cylinder juncture, the negative shift in step base pressure coefficient near sonic speeds is noticeably more abrupt and is greatly increased compared with that for the typical launch-vehicle base step. For example, for the 15° nose-cone configuration having a fineness ratio of 0.5 (fig. 11), the step base pressure coefficient varies from about -0.14 at a Mach number of 0.85 to about -0.80 at a Mach number of 0.95 or by an increment roughly five times that associated with the launch-vehicle configuration. Examination of results presented for the 30° half-angle nose-cone configurations in figure 11 indicates that as the nose angle is increased, the severity of the pressure variations increases somewhat.

These severe and abrupt variations in pressure coefficient, considered in the light of typical Mach number and dynamic-pressure time variations for actual flight, suggest that significant venting problems may occur with the use of step base venting, where the bases are located within rapidly varying pressure fields.

CONCLUDING REMARKS

An investigation conducted at transonic speeds to determine the effects of step height and location on rearward-facing-step base pressures has indicated the following results:

For a typical launch-vehicle model used to simulate the case where the step was located at a considerable distance downstream of the nose-cone—cylinder juncture, step base pressure coefficients were found to be relatively insensitive to variations in Reynolds number. Slight effects of Reynolds number were noted, however, both in the cylinder surface pressures preceding a step and in the step base pressure coefficients for a configuration simulating the case where the step was located close to a nose-cone—cylinder juncture.

For both 15° and 30° nose-cone—cylinder models, locating the step within the influence of the pressure fields associated with the nose-cone—cylinder junctures resulted in step base pressure variations with Mach number which were considerably more abrupt and about five times more severe than those for the case where the step was located several body diameters downstream of the juncture.

In general, the variation of step base pressure coefficient with variation in step height was relatively gradual for all configurations.

Significant effects of transition-strip location were noted for a 30° nose-cone—cylinder configuration which served to emphasize the need for careful

application of such strips in order to obtain accurate measurements of the local distributed loads for scaled launch-vehicle models.

Langley Research Center,
National Aeronautics and Space Administration,
Langley Station, Hampton, Va., April 5, 1965.

REFERENCES

1. Chapman, Dean R.: An Analysis of Base Pressure at Supersonic Velocities and Comparison With Experiment. NACA Rept. 1051, 1951. (Supersedes NACA TN 2137.)

2. Korst, H. H.; Page, R. H.; and Childs, M. E.: A Theory for Base Pressures in Transonic and Supersonic Flow. M.E. Tech. Note 392-2 (Contract No. AF 18(600)-392), Eng. Expt. Sta., Univ. of Illinois, Mar. 1955.

3. Lee, George; and Summers, James L.: Effects of Sting-Support Interference on the Drag of an Ogive-Cylinder Body With and Without a Boattail at 0.6 to 1.4 Mach Number. NACA RM A57I09, 1957.

4. Love, Eugene S.: A Summary of Information on Support Interference at Transonic and Supersonic Speeds. NACA RM L53K12, 1954.

TABLE I.- SUMMARY OF CONFIGURATION CHARACTERISTICS

Nose half-angle, deg	Cylinder fineness ratio, l/D	Step ratio d/D	Configuration designation
Typical launch vehicle			
----	---	0.713	111
----	---	.832	112
----	---	.910	113
----	---	.952	114
Cone-cylinder configuration			
15.0	1.0	0.832	122
15.0	1.0	.910	123
15.0	1.0	.952	124
15.0	1.0	1.0	125
30.0	1.0	.952	224
30.0	1.0	1.0	225
15.0	.5	.952	134
30.0	.5	.952	234

TABLE II.- STEP BASE PRESSURE COEFFICIENTS FOR

LAUNCH-VEHICLE MODELS

(a) Configuration 111; d/D = 0.713; $R_{ft} = 4.0 \times 10^6$

Mach number	$C_{p,b}$ for orifice at ϕ of -						Average $C_{p,b}$
	0°	45°	90°	135°	180°	270°	
0.40	-0.132	-0.132	-0.132	-0.132	-0.132	-0.132	-0.132
.60	-.122	-.119	-.119	-.119	-.119	-.119	-.120
.80	-.120	-.120	-.120	-.120	-.120	-.120	-.120
.90	-.139	-.142	-.142	-.139	-.142	-.142	-.141
.95	-.133	-.133	-.133	-.133	-.133	-.133	-.133
1.00	-.233	-.233	-.233	-.233	-.233	-.235	-.233
1.025	-.268	-.270	-.270	-.268	-.268	-.270	-.269
1.10	-.258	-.258	-.258	-.258	-.258	-.254	-.257
1.20	-.220	-.220	-.220	-.220	-.218	-.218	-.219

(b) Configuration 112; d/D = 0.832; $R_{ft} = 4.0 \times 10^6$

Mach number	$C_{p,b}$ for orifice at ϕ of -						Average $C_{p,b}$
	0°	45°	90°	135°	180°	270°	
0.40	-0.119	-0.119	-0.119	-0.119	-0.119	-0.119	-0.119
.60	-.115	-.118	-.115	-.118	-.118	-.115	-.116
.80	-.121	-.123	-.121	-.123	-.123	-.123	-.122
.90	-.100	-.102	-.100	-.102	-.102	-.102	-.101
.95	-.161	-.161	-.159	-.161	-.161	-.161	-.161
1.00	-.251	-.251	-.249	-.251	-.251	-.251	-.251
1.025	-.291	-.291	-.289	-.291	-.292	-.291	-.291
1.10	-.273	-.273	-.271	-.273	-.273	-.273	-.273
1.20	-.235	-.235	-.233	-.235	-.235	-.235	-.235

TABLE II.- STEP BASE PRESSURE COEFFICIENTS FOR

LAUNCH-VEHICLE MODELS - Continued

(c) Configuration 112; d/D = 0.832; $R_{ft} = 2.0 \times 10^6$

Mach number	$C_{p,b}$ for orifice at ϕ of -						Average $C_{p,b}$
	0°	45°	90°	135°	180°	270°	
0.40	-0.107	-0.107	-0.107	-0.107	-0.107	-0.107	-0.107
.60	-.114	-.114	-.114	-.114	-.114	-.114	-.114
.80	-.120	-.124	-.124	-.124	-.124	-.124	-.123
1.00	-.190	-.190	-.190	-.190	-.190	-.190	-.190
1.20	-.250	-.250	-.250	-.254	-.250	-.254	-.251

(d) Configuration 113; d/D = 0.910; $R_{ft} = 4.0 \times 10^6$

Mach number	$C_{p,b}$ for orifice at ϕ of -						Average $C_{p,b}$
	0°	45°	90°	135°	180°	270°	
0.40	-0.107	-0.107	-0.107	-0.107	-0.107	-0.107	-0.107
.60	-.113	-.113	-.110	-.110	-.113	-.110	-.111
.80	-.112	-.114	-.112	-.109	-.109	-.109	-.111
.90	-.135	-.137	-.133	-.133	-.133	-.133	-.134
.95	-.197	-.197	-.199	-.193	-.195	-.195	-.196
1.00	-.265	-.265	-.263	-.261	-.261	-.261	-.263
1.025	-.292	-.291	-.289	-.287	-.289	-.287	-.289
1.05	-.225	-.227	-.223	-.223	-.223	-.221	-.224
1.10	-.261	-.263	-.260	-.258	-.260	-.260	-.260
1.20	-.239	-.239	-.237	-.235	-.237	-.237	-.237

TABLE II.- STEP BASE PRESSURE COEFFICIENTS FOR

LAUNCH-VEHICLE MODELS - Concluded

(e) Configuration 114; d/D = 0.952; $R_{ft} = 4.0 \times 10^6$

Mach number	$C_{p,b}$ for orifice at ϕ of -						Average $C_{p,b}$
	0°	45°	90°	135°	180°	270°	
0.40	-0.092	-0.096	-0.092	-0.092	-0.092	-0.092	-0.093
.60	-.098	-.095	-.095	-.095	-.095	-.092	-.095
.80	-.095	-.099	-.095	-.099	-.097	-.092	-.096
.90	-.110	-.115	-.113	-.113	-.113	-.108	-.112
.95	-.106	-.111	-.109	-.109	-.109	-.104	-.108
1.00	-.206	-.212	-.208	-.210	-.210	-.204	-.208
1.025	-.242	-.246	-.242	-.244	-.244	-.238	-.243
1.10	-.239	-.242	-.240	-.240	-.240	-.237	-.240
1.20	-.217	-.220	-.218	-.218	-.218	-.217	-.218

(f) Configuration 114; d/D = 0.952; $R_{ft} = 2.0 \times 10^6$

Mach number	$C_{p,b}$ for orifice at ϕ of -						Average $C_{p,b}$
	0°	45°	90°	135°	180°	270°	
0.40	-0.099	-0.099	-0.099	-0.099	-0.099	-0.099	-0.099
.60	-.093	-.096	-.093	-.093	-.090	-.090	-.092
.80	-.097	-.102	-.097	-.100	-.097	-.095	-.098
.90	-.113	-.120	-.115	-.118	-.115	-.113	-.116
.95	-.127	-.131	-.129	-.129	-.129	-.125	-.128
1.00	-.204	-.200	-.202	-.202	-.202	-.192	-.200
1.10	-.231	-.235	-.229	-.229	-.229	-.227	-.230
1.20	-.206	-.210	-.206	-.206	-.206	-.202	-.206

TABLE III.- STEP BASE PRESSURE COEFFICIENTS FOR CONE-CYLINDER MODELS

(a) Configuration 122; $\delta_N = 15^\circ$; $l/D = 1.0$; $d/D = 0.832$; $R_{ft} = 4.0 \times 10^6$; single transition strip

Mach number	$C_{p,b}$ for orifice at ϕ of -				Average $C_{p,b}$
	0°	90°	180°	270°	
0.40	-0.181	-0.181	-0.176	-0.181	-0.180
.60	-.180	-.180	-.177	-.180	-.179
.80	-.194	-.194	-.192	-.194	-.194
.90	-.132	-.132	-.130	-.132	-.132
.95	-.279	-.277	-.275	-.279	-.278
1.00	-.465	-.465	-.463	-.467	-.465
1.025	-.429	-.427	-.425	-.429	-.428
1.10	-.404	-.402	-.400	-.404	-.403
1.20	-.361	-.361	-.357	-.361	-.360

(b) Configuration 123; $\delta_N = 15^\circ$; $l/D = 1.0$; $d/D = 0.910$; $R_{ft} = 4.0 \times 10^6$; single transition strip

Mach number	$C_{p,b}$ for orifice at ϕ of -				Average $C_{p,b}$
	0°	90°	180°	270°	
0.40	-0.180	-0.180	-0.180	-0.180	-0.180
.60	-.177	-.177	-.177	-.180	-.178
.80	-.199	-.199	-.197	-.199	-.199
.85	-.194	-.192	-.192	-.194	-.193
.90	-.120	-.120	-.118	-.118	-.119
.95	-.337	-.335	-.333	-.335	-.335
1.00	-.505	-.501	-.501	-.503	-.503
1.025	-.468	-.466	-.466	-.468	-.467
1.10	-.435	-.433	-.433	-.435	-.434
1.20	-.386	-.385	-.383	-.386	-.385

TABLE III.- STEP BASE PRESSURE COEFFICIENTS FOR

CONE-CYLINDER MODELS - Continued

(c) Configuration 124; $\delta_N = 15^\circ$; $l/D = 1.0$; $d/D = 0.952$; $R_{ft} = 4.0 \times 10^6$; single transition strip

Mach number	$C_{p,b}$ for orifice at ϕ of -				Average $C_{p,b}$
	0°	90°	180°	270°	
0.40	-0.166	-0.166	-0.166	-0.162	-0.165
.60	-.166	-.166	-.166	-.160	-.165
.80	-.180	-.180	-.182	-.178	-.180
.85	-.176	-.178	-.181	-.172	-.177
.90	-.094	-.096	-.096	-.090	-.094
.95	-.474	-.474	-.476	-.464	-.472
1.00	-.521	-.521	-.523	-.515	-.520
1.025	-.480	-.480	-.480	-.474	-.479
1.10	-.448	-.446	-.446	-.443	-.446
1.20	-.390	-.388	-.390	-.385	-.388

(d) Configuration 124; $\delta_N = 15^\circ$; $l/D = 1.0$; $d/D = 0.952$; $R_{ft} = 2.0 \times 10^6$; single transition strip

Mach number	$C_{p,b}$ for orifice at ϕ of -				Average $C_{p,b}$
	0°	90°	180°	270°	
0.40	-0.169	-0.178	-0.178	-0.169	-0.174
.60	-.170	-.170	-.175	-.170	-.171
.80	-.178	-.182	-.187	-.178	-.181
1.00	-.532	-.532	-.532	-.520	-.529
1.20	-.390	-.390	-.390	-.382	-.388

TABLE III.- STEP BASE PRESSURE COEFFICIENTS FOR

CONE-CYLINDER MODELS - Continued

(e) Configuration 132; $\delta_N = 15^\circ$; $l/D = 0.5$; $d/D = 0.952$; $R_{ft} = 4.0 \times 10^6$; single transition strip

Mach number	$C_{p,b}$ for orifice at ϕ of -				Average $C_{p,b}$
	0°	90°	180°	270°	
0.40	-0.211	-0.207	-0.207	-0.211	-0.209
.60	-.183	-.180	-.180	-.180	-.181
.80	-.225	-.225	-.223	-.225	-.225
.85	-.135	-.137	-.135	-.133	-.135
.90	-.253	-.255	-.248	-.246	-.251
.95	-.796	-.794	-.794	-.794	-.795
1.00	-.709	-.709	-.707	-.709	-.709
1.025	-.661	-.659	-.659	-.659	-.660
1.10	-.581	-.579	-.579	-.579	-.579
1.20	-.490	-.488	-.488	-.488	-.489

(f) Configuration 224; $\delta_N = 30^\circ$; $l/D = 1.0$; $d/D = 0.952$; $R_{ft} = 4.0 \times 10^6$; double transition strips

Mach number	$C_{p,b}$ for orifice at ϕ of -				Average $C_{p,b}$
	0°	90°	180°	270°	
0.40	-0.174	-0.174	-0.170	-0.170	-0.172
.60	-.147	-.144	-.153	-.150	-.149
.70	-.105	-.105	-.105	-.105	-.105
.80	-.125	-.118	-.121	-.123	-.122
.85	-.188	-.188	-.184	-.184	-.186
.90	-.069	-.056	-.077	-.073	-.069
.95	-.488	-.502	-.479	-.475	-.486
1.00	-.572	-.568	-.572	-.564	-.569
1.025	-.528	-.524	-.528	-.520	-.525
1.10	-.490	-.485	-.489	-.483	-.487
1.20	-.436	-.430	-.434	-.428	-.432

TABLE III.- STEP BASE PRESSURE COEFFICIENTS FOR

CONE-CYLINDER MODELS - Concluded

(g) Configuration 234; $\delta_N = 30^\circ$; $l/D = 0.5$; $d/D = 0.952$; $R_{ft} = 4.0 \times 10^6$; double transition strips

Mach number	$C_{p,b}$ for orifice at ϕ of -				Average $C_{p,b}$
	0°	90°	180°	270°	
0.40	-0.247	-0.247	-0.247	-0.247	-0.247
.60	-.205	-.208	-.208	-.205	-.207
.70	-.241	-.241	-.244	-.244	-.243
.80	-.407	-.398	-.410	-.421	-.409
.85	-.461	-.442	-.468	-.470	-.460
.90	-.465	-.448	-.439	-.465	-.454
.95	-.944	-.950	-.940	-.944	-.945
1.00	-.837	-.833	-.833	-.839	-.836
1.025	-.781	-.775	-.777	-.783	-.779
1.10	-.690	-.686	-.688	-.692	-.689
1.20	-.576	-.572	-.572	-.576	-.574

TABLE IV.- SURFACE PRESSURE COEFFICIENTS FOR

CONE-CYLINDER MODELS

(a) Configuration 122; $\delta_N = 15^\circ$; $l/D = 1.0$; $d/D = 0.832$; $R_{ft} = 4.0 \times 10^6$; single transition strip

Mach number	C_p for orifice at x/D of -						
	0.029	0.181	0.342	0.503	0.665	0.819	0.958
0.40	-0.529	-0.207	-0.137	-0.110	-0.101	-0.106	-0.150
.60	-.591	-.217	-.139	-.110	-.099	-.104	-.148
.80	-1.287	-.380	-.100	-.088	-.093	-.102	-.157
.90	-.974	-.846	-.699	-.573	-.152	-.038	-.081
.95	-.839	-.733	-.610	-.521	-.442	-.372	-.320
1.00	-.721	-.625	-.513	-.435	-.367	-.305	-.293
1.025	-.666	-.573	-.464	-.387	-.320	-.261	-.249
1.10	-.533	-.458	-.369	-.308	-.260	-.213	-.202
1.20	-.388	-.332	-.264	-.220	-.183	-.154	-.143

(b) Configuration 123; $\delta_N = 15^\circ$; $l/D = 1.0$; $d/D = 0.910$; $R_{ft} = 4.0 \times 10^6$; single transition strip

Mach number	C_p for orifice at x/D of -						
	0.029	0.181	0.342	0.503	0.665	0.819	0.958
0.40	-0.526	-0.202	-0.132	-0.105	-0.092	-0.096	-0.145
.60	-.587	-.212	-.134	-.105	-.093	-.096	-.142
.80	-1.285	-.373	-.100	-.083	-.086	-.095	-.153
.85	-1.115	-.943	-.212	-.038	-.040	-.068	-.141
.90	-.968	-.840	-.694	-.568	-.137	-.028	-.071
.95	-.841	-.733	-.613	-.524	-.443	-.373	-.337
1.00	-.713	-.619	-.509	-.427	-.359	-.299	-.287
1.025	-.664	-.571	-.462	-.385	-.318	-.261	-.249
1.10	-.519	-.447	-.359	-.302	-.253	-.209	-.198
1.20	-.388	-.332	-.264	-.220	-.183	-.152	-.143

TABLE IV.- SURFACE PRESSURE COEFFICIENTS FOR

CONE-CYLINDER MODELS - Continued

(c) Configuration 124; $\delta_N = 15^\circ$; $l/D = 1.0$; $d/D = 0.952$; $R_{ft} = 4.0 \times 10^6$; single transition strip

Mach number	C_p for orifice at x/D of -						
	0.029	0.181	0.342	0.503	0.665	0.819	0.958
0.40	-0.533	-0.192	-0.127	-0.096	-0.087	-0.083	-0.127
.60	-.590	-.206	-.131	-.099	-.084	-.081	-.125
.80	-1.279	-.356	-.095	-.079	-.074	-.079	-.134
.85	-1.108	-.934	-.227	-.035	-.029	-.053	-.123
.90	-.966	-.833	-.695	-.557	-.117	-.015	-.049
.95	-.833	-.724	-.608	-.520	-.439	-.369	-.355
1.00	-.725	-.625	-.519	-.439	-.369	-.305	-.297
1.025	-.670	-.571	-.468	-.391	-.324	-.263	-.253
1.10	-.536	-.458	-.374	-.314	-.264	-.216	-.209
1.20	-.390	-.330	-.266	-.222	-.183	-.152	-.145

(d) Configuration 124; $\delta_N = 15^\circ$; $l/D = 1.0$; $d/D = 0.952$; $R_{ft} = 2.0 \times 10^6$; single transition strip

Mach number	C_p for orifice at x/D of -						
	0.029	0.181	0.342	0.503	0.665	0.819	0.958
0.40	-0.534	-0.203	-0.136	-0.110	-0.093	-0.093	-0.136
.60	-.713	-.222	-.140	-.105	-.094	-.088	-.135
.80	-1.280	-.383	-.126	-.089	-.079	-.084	-.140
1.00	-.726	-.641	-.536	-.448	-.379	-.315	-.306
1.20	-.379	-.331	-.272	-.221	-.184	-.151	-.147

TABLE IV.- SURFACE PRESSURE COEFFICIENTS FOR

CONE-CYLINDER MODELS - Continued

(e) Configuration 125; $\delta_N = 15°$; $l/D = \infty$; $d/D = 1.0$;
$R_{ft} = 4.0 \times 10^6$; single transition strip

Mach number	C_p for orifice at x/D of -						
	0.029	0.181	0.342	0.503	0.665	0.819	0.958
0.40	-0.514	-0.190	-0.116	-0.088	-0.065	-0.051	-0.046
.60	-.566	-.190	-.107	-.072	-.052	-.038	-.032
.80	-1.282	-.354	-.081	-.060	-.049	-.037	-.035
.85	-1.117	-.949	-.178	-.015	-.011	-.018	-.022
.90	-.970	-.814	-.694	-.353	-.041	.034	.041
.95	-.841	-.710	-.615	-.528	-.447	-.377	-.325
1.00	-.723	-.604	-.516	-.440	-.369	-.307	-.267
1.025	-.666	-.551	-.464	-.395	-.324	-.265	-.229
1.10	-.533	-.437	-.372	-.314	-.262	-.218	-.193
1.20	-.391	-.312	-.266	-.224	-.187	-.152	-.141

(f) Configuration 125; $\delta_N = 15°$; $l/D = \infty$; $d/D = 1.0$;
$R_{ft} = 4.0 \times 10^6$; double transition strips

Mach number	C_p for orifice at x/D of -						
	0.029	0.181	0.342	0.503	0.665	0.819	0.958
0.40	-0.556	-0.190	-0.111	-0.079	-0.056	-0.046	-0.042
.60	-.694	-.202	-.110	-.078	-.055	-.040	-.038
.80	-1.213	-.419	-.134	-.076	-.056	-.044	-.039
.85	-1.057	-.921	-.214	-.064	-.026	-.024	-.029
.90	-.915	-.848	-.694	-.376	-.071	.011	.028
.95	-.787	-.739	-.609	-.526	-.445	-.375	-.329
1.00	-.671	-.631	-.513	-.441	-.371	-.311	-.279
1.025	-.615	-.575	-.462	-.391	-.324	-.265	-.237
1.10	-.486	-.461	-.367	-.314	-.262	-.218	-.197
1.20	-.350	-.338	-.264	-.224	-.189	-.158	-.144

TABLE IV.- SURFACE PRESSURE COEFFICIENTS FOR

CONE-CYLINDER MODELS - Continued

(g) Configuration 134; $\delta_N = 15^\circ$; $l/D = 0.5$; $d/D = 0.952$; $R_{ft} = 4.0 \times 10^6$; single transition strip

Mach number	C_p for orifice at x/D of -			
	0.032	0.181	0.345	0.461
0.40	-0.520	-0.207	-0.154	-0.172
.60	-.577	-.220	-.159	-.177
.80	-1.285	-.397	-.118	-.162
.85	-1.118	-.953	-.251	-.115
.90	-.968	-.842	-.696	-.462
.95	-.827	-.724	-.604	-.534
1.00	-.713	-.621	-.511	-.447
1.025	-.659	-.570	-.463	-.402
1.10	-.524	-.453	-.369	-.319
1.20	-.382	-.328	-.266	-.229

(h) Configuration 224; $\delta_N = 30^\circ$; $l/D = 1.0$; $d/D = 0.952$; $R_{ft} = 4.0 \times 10^6$; double transition strips

Mach number	C_p for orifice at x/D of -						
	0.029	0.181	0.342	0.503	0.665	0.819	0.958
0.40	-1.326	-0.374	-0.187	-0.130	-0.113	-0.104	-0.135
.60	-1.133	-.697	-.317	-.156	-.095	-.084	-.112
.70	-.900	-.769	-.544	-.308	-.158	-.090	-.078
.80	-.796	-.766	-.652	-.513	-.362	-.225	-.137
.85	-.916	-.758	-.665	-.554	-.439	-.322	-.224
.90	-1.234	-1.210	-1.026	-.820	-.373	-.191	-.086
.95	-1.070	-1.056	-.888	-.736	-.614	-.498	-.446
1.00	-1.074	-.928	-.773	-.643	-.526	-.430	-.384
1.025	-1.014	-.870	-.717	-.591	-.478	-.385	-.340
1.10	-.860	-.734	-.603	-.496	-.398	-.322	-.280
1.20	-.682	-.586	-.478	-.390	-.313	-.252	-.217

TABLE IV.- SURFACE PRESSURE COEFFICIENTS FOR

CONE-CYLINDER MODEL - Continued

(i) Configuration 225; $\delta_N = 30^\circ$; $l/D = 1.0$; $d/D = 1.0$;

$R_{ft} = 4.0 \times 10^6$; single transition strip

Mach number	C_p for orifice at x/D of -						
	0.029	0.181	0.342	0.503	0.665	0.819	0.958
0.40	-0.769	-0.773	-0.403	-0.093	-0.037	-0.028	-0.028
.60	-.620	-.643	-.632	-.461	-.180	-.049	.006
.80	-.521	-.528	-.542	-.551	-.523	-.447	-.350
.85	-.526	-.533	-.544	-.555	-.546	-.504	-.443
.90	-.561	-.563	-.572	-.580	-.567	-.529	-.480
*.90	-1.370	-1.221	-1.015	-.850	-.469	-.152	-.028
.95	-1.213	-1.079	-.894	-.749	-.621	-.511	-.439
1.00	-1.076	-.950	-.779	-.645	-.528	-.430	-.365
1.025	-1.010	-.887	-.721	-.591	-.478	-.383	-.325
1.10	-.856	-.747	-.603	-.490	-.397	-.316	-.266
1.20	-.692	-.604	-.483	-.394	-.317	-.257	-.217

*Mach number decreasing.

(j) Configuration 225; $\delta_N = 30^\circ$; $l/D = 1.0$; $d/D = 1.0$;

$R_{ft} = 4.0 \times 10^6$; double transition strips

Mach number	C_p for orifice at x/D of -						
	0.029	0.181	0.342	0.503	0.665	0.819	0.958
0.40	-1.310	-0.352	-0.162	-0.106	-0.074	-0.056	-0.046
.60	-1.110	-.701	-.304	-.139	-.084	-.061	-.052
.80	-.810	-.752	-.653	-.505	-.347	-.208	-.116
.85	-1.073	-.779	-.669	-.539	-.408	-.289	-.194
.90	-1.389	-1.212	-1.011	-.835	-.340	-.154	-.032
.95	-1.227	-1.072	-.895	-.752	-.624	-.514	-.442
1.00	-1.092	-.946	-.783	-.653	-.534	-.436	-.376
1.025	-1.030	-.887	-.725	-.597	-.486	-.389	-.330
1.10	-.872	-.746	-.606	-.495	-.402	-.321	-.273
1.20	-.697	-.591	-.473	-.387	-.312	-.248	-.207

TABLE IV.- SURFACE PRESSURE COEFFICIENTS FOR

CONE-CYLINDER MODELS - Concluded

(k) Configuration 234; $\delta_N = 30^\circ$; $l/D = 0.5$; $d/D = 0.952$; $R_{ft} = 4.0 \times 10^6$; double transition strips

Mach number	C_p for orifice at x/D of -			
	0.032	0.181	0.345	0.461
0.40	-1.251	-0.377	-0.216	-0.216
.60	-1.205	-.650	-.263	-.194
.70	-1.123	-.781	-.462	-.284
.80	-1.016	-.775	-.616	-.484
.85	-.976	-.740	-.638	-.547
.90	-1.437	-1.111	-.689	-.518
.95	-1.303	-1.064	-.894	-.786
1.00	-1.070	-.950	-.779	-.671
1.025	-1.002	-.885	-.719	-.617
1.10	-.849	-.745	-.598	-.506
1.20	-.673	-.583	-.462	-.387

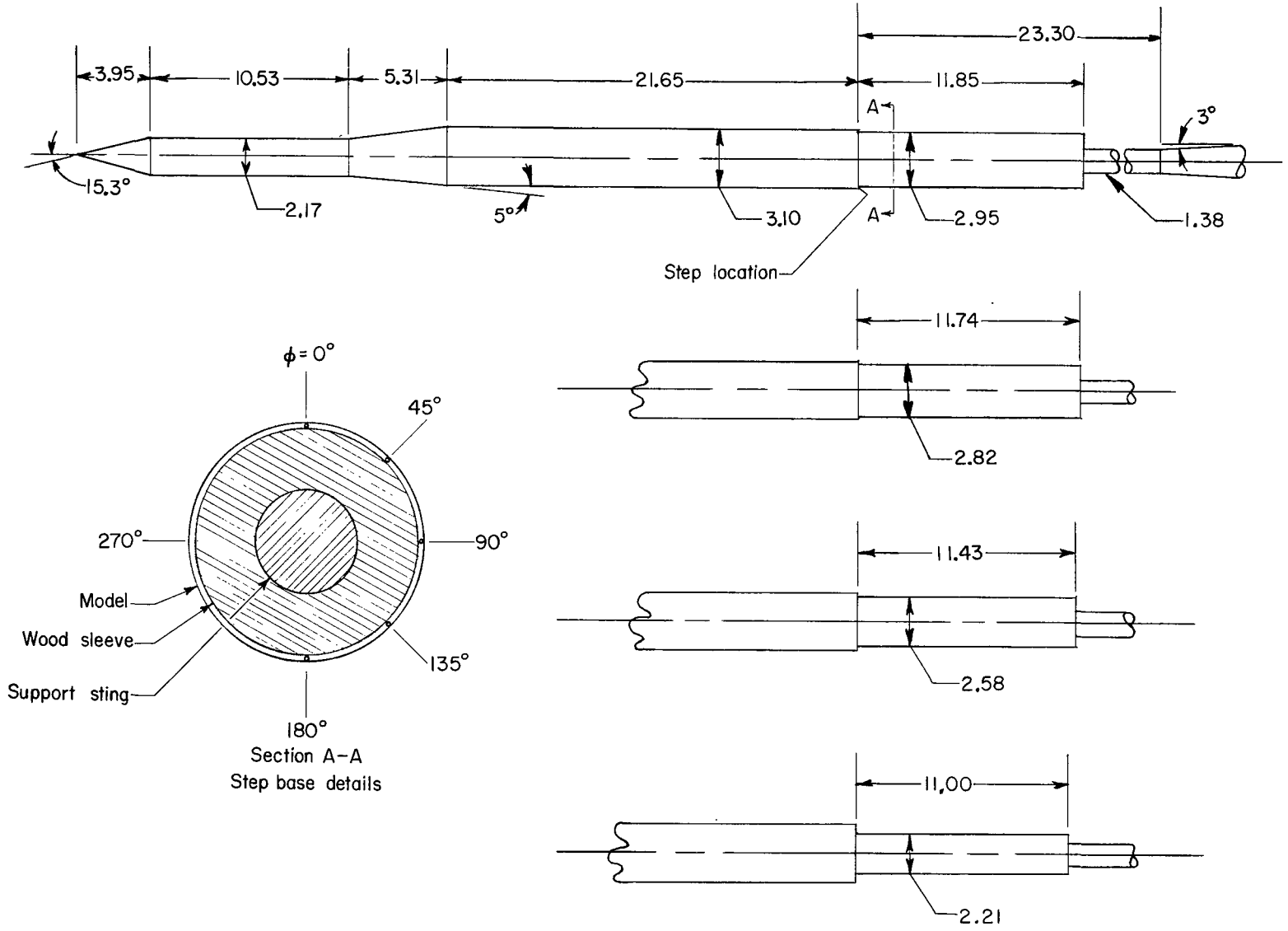

(a) Typical launch-vehicle configurations.

Figure 1.- Model configurations. All dimensions are in inches unless otherwise noted.

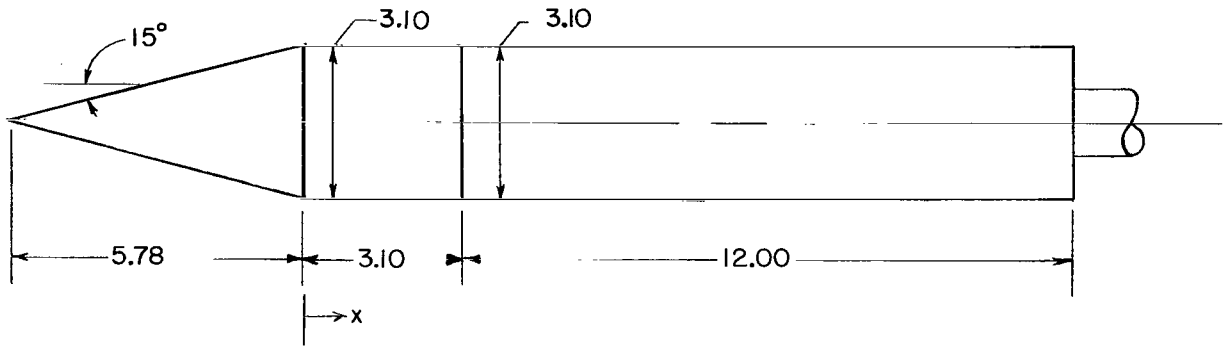

Orifice locations

x, in.	x/D
0.09	0.029
.56	.181
1.06	.342
1.56	.503
2.06	.665
2.54	.819
2.97	.958

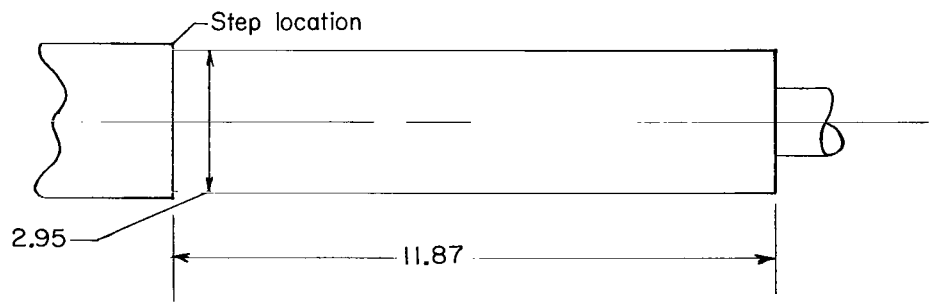

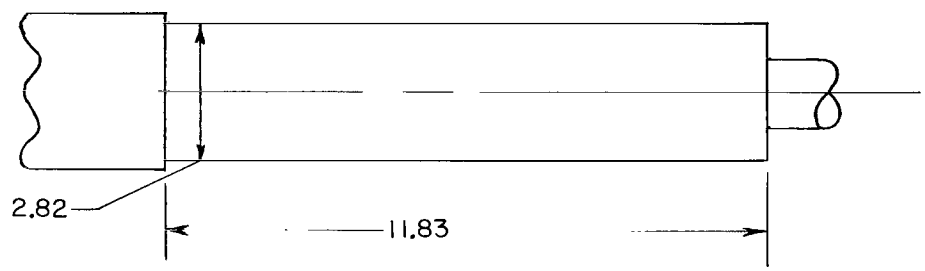

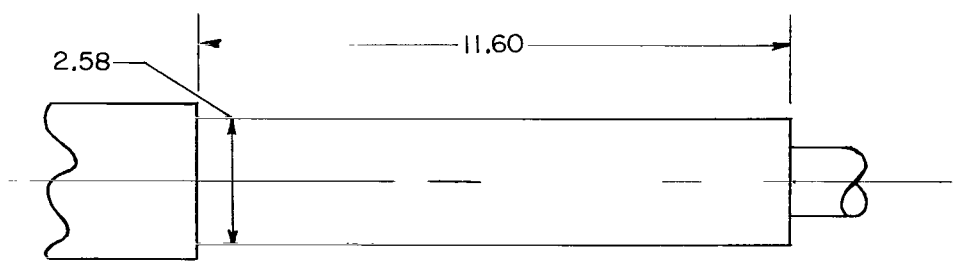

(b) Nose-cone—cylinder configurations. Fineness ratio = 1.0; $\delta_N = 15^0$.

Figure 1.- Continued.

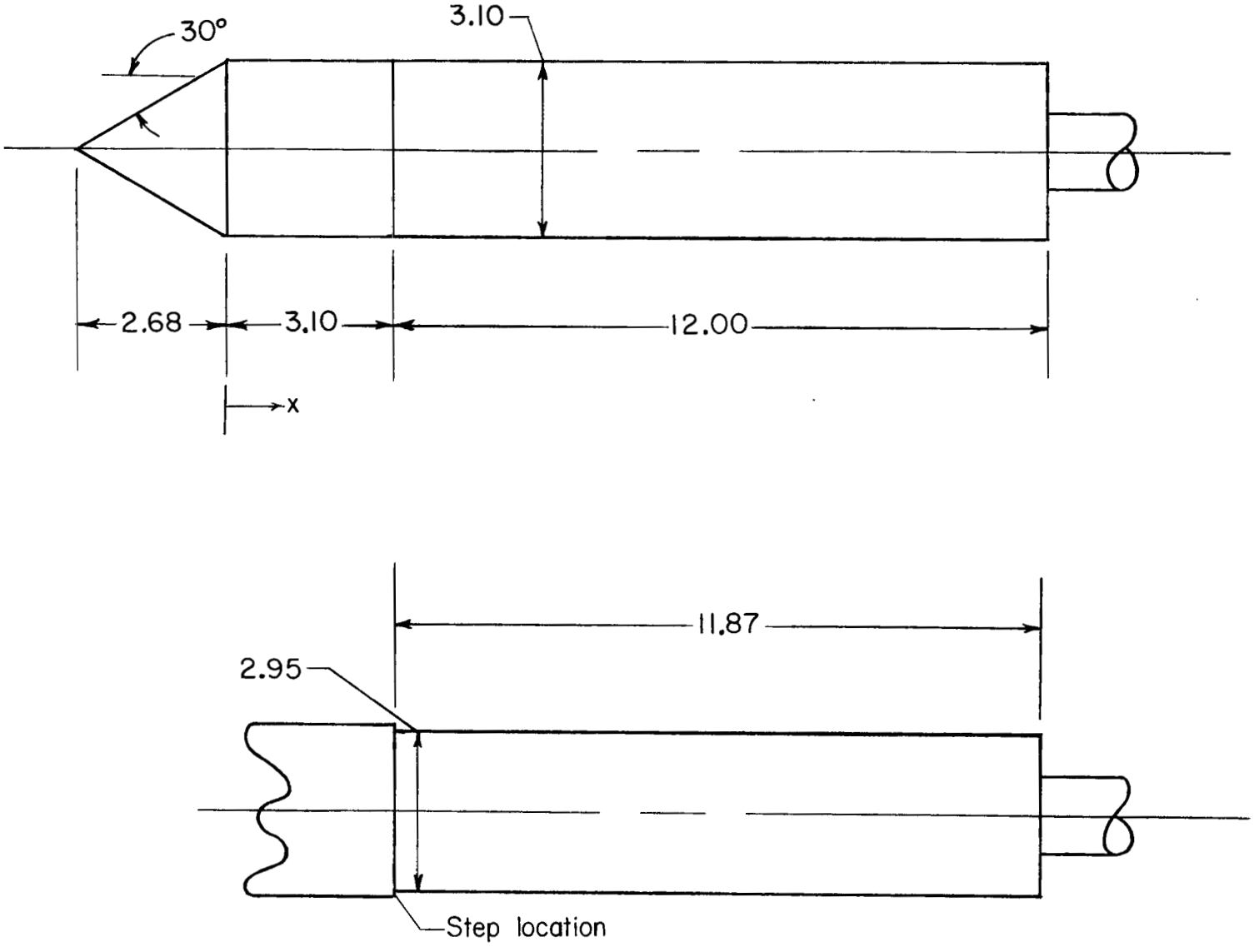

(c) Nose-cone—cylinder configurations. Fineness ratio = 1.0; $\delta_N = 30^0$.

Figure 1.- Continued.

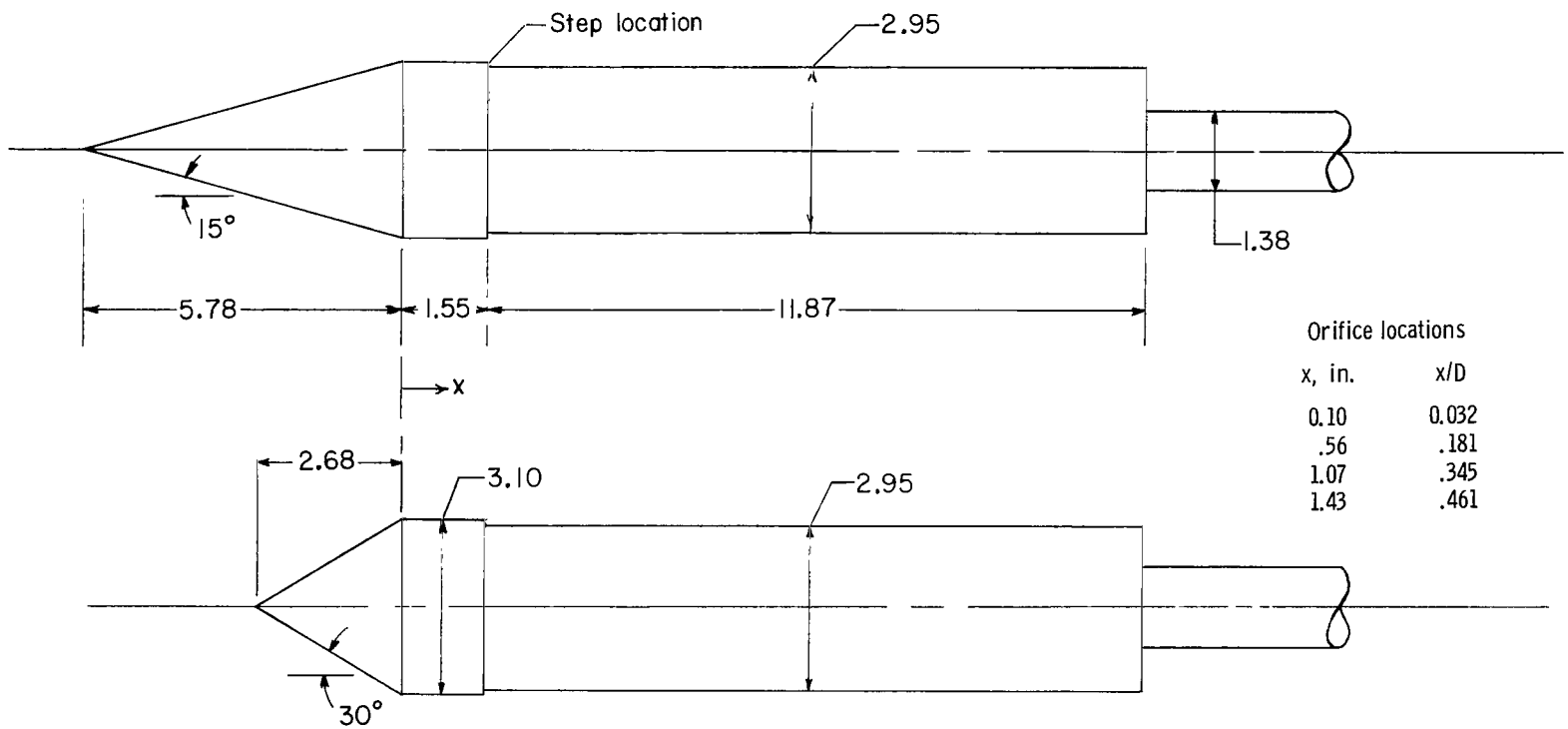

(d) Nose-cone—cylinder configurations. Fineness ratio = 0.5.

Figure 1.- Concluded.

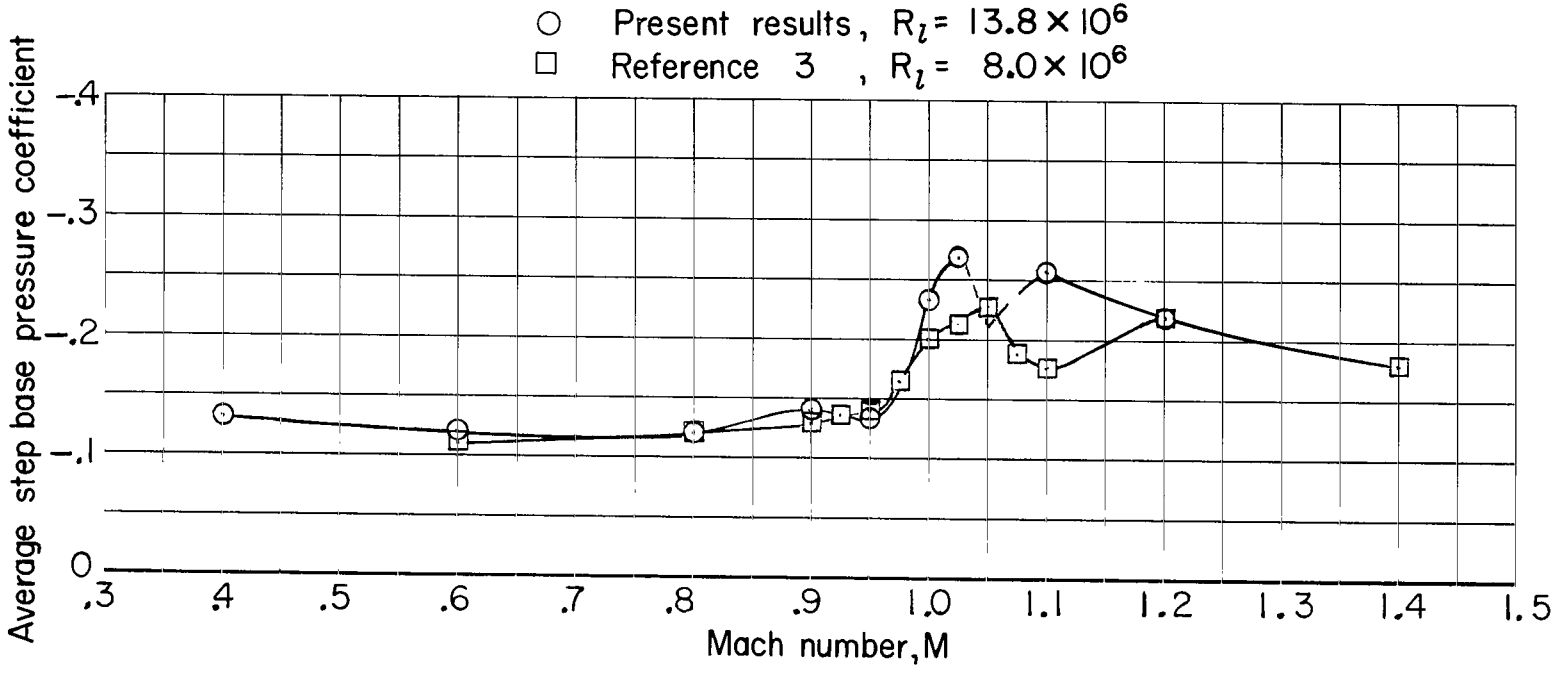

Figure 2.- Variation of average step base pressure coefficient with Mach number for launch-vehicle models. d/D = 0.713.

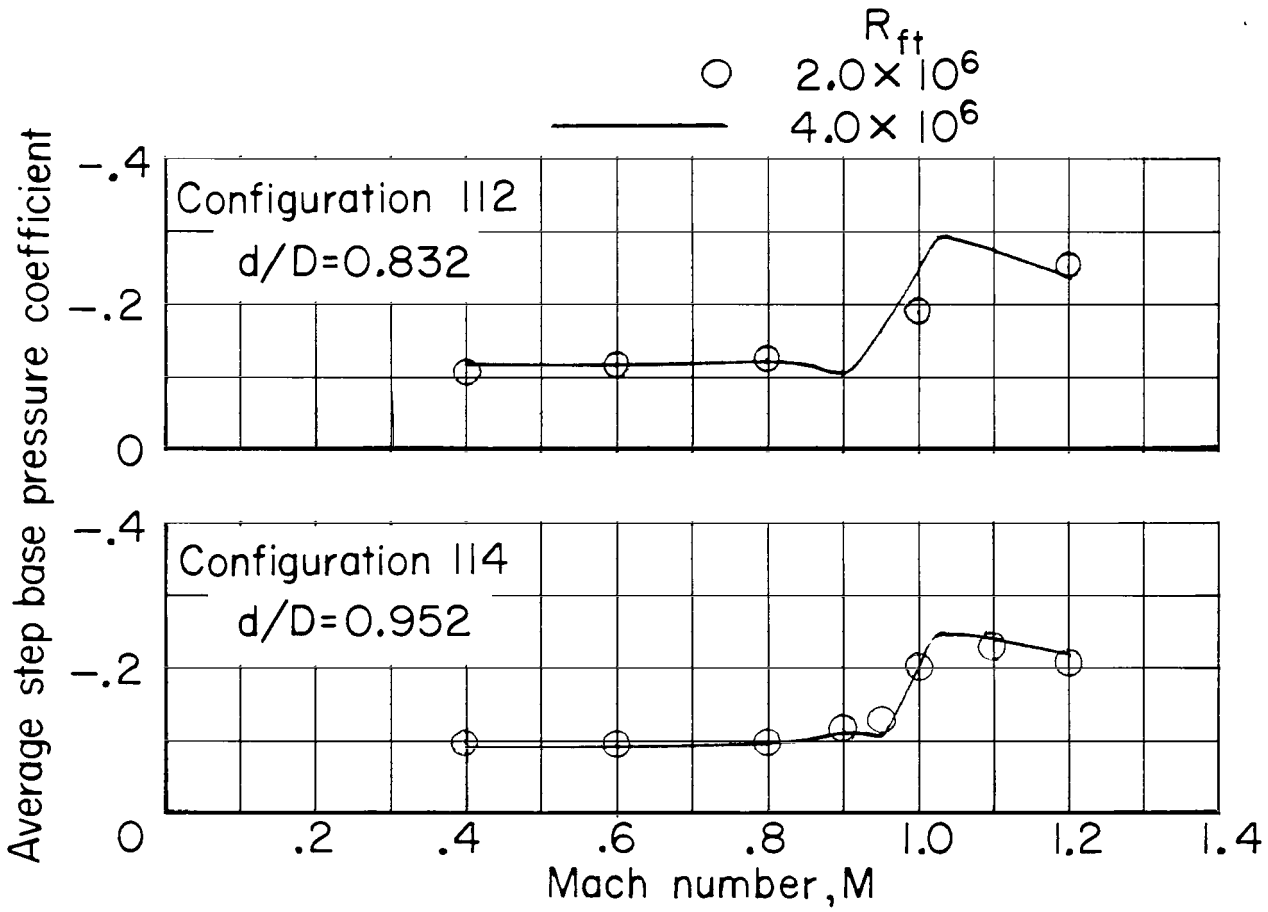

Figure 3.- Effect of Reynolds number on average step base pressure coefficients for typical launch-vehicle models.

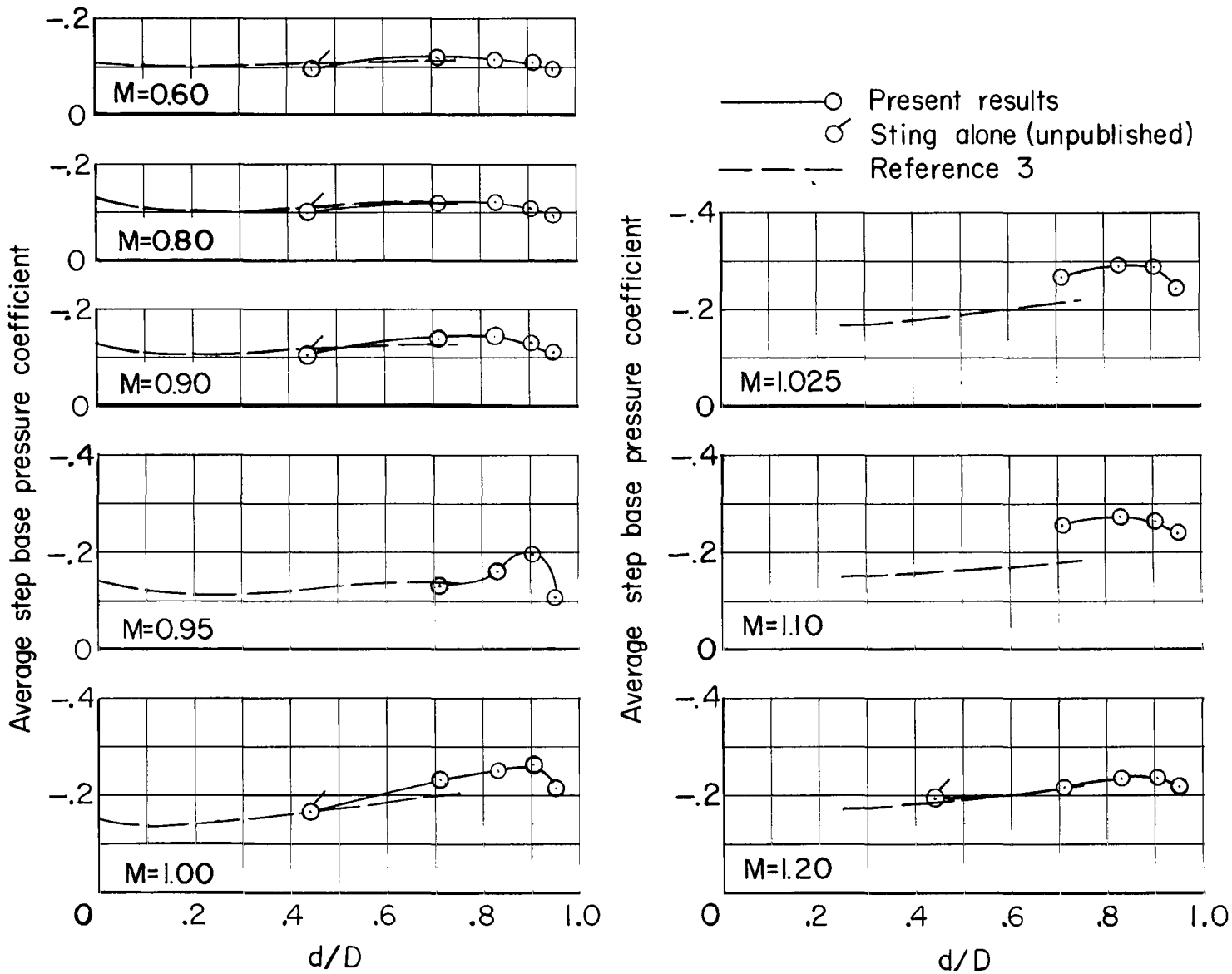

Figure 4.- Effect of step height on average step base pressure coefficients for typical launch-vehicle model. $R_{ft} = 4.0 \times 10^6$.

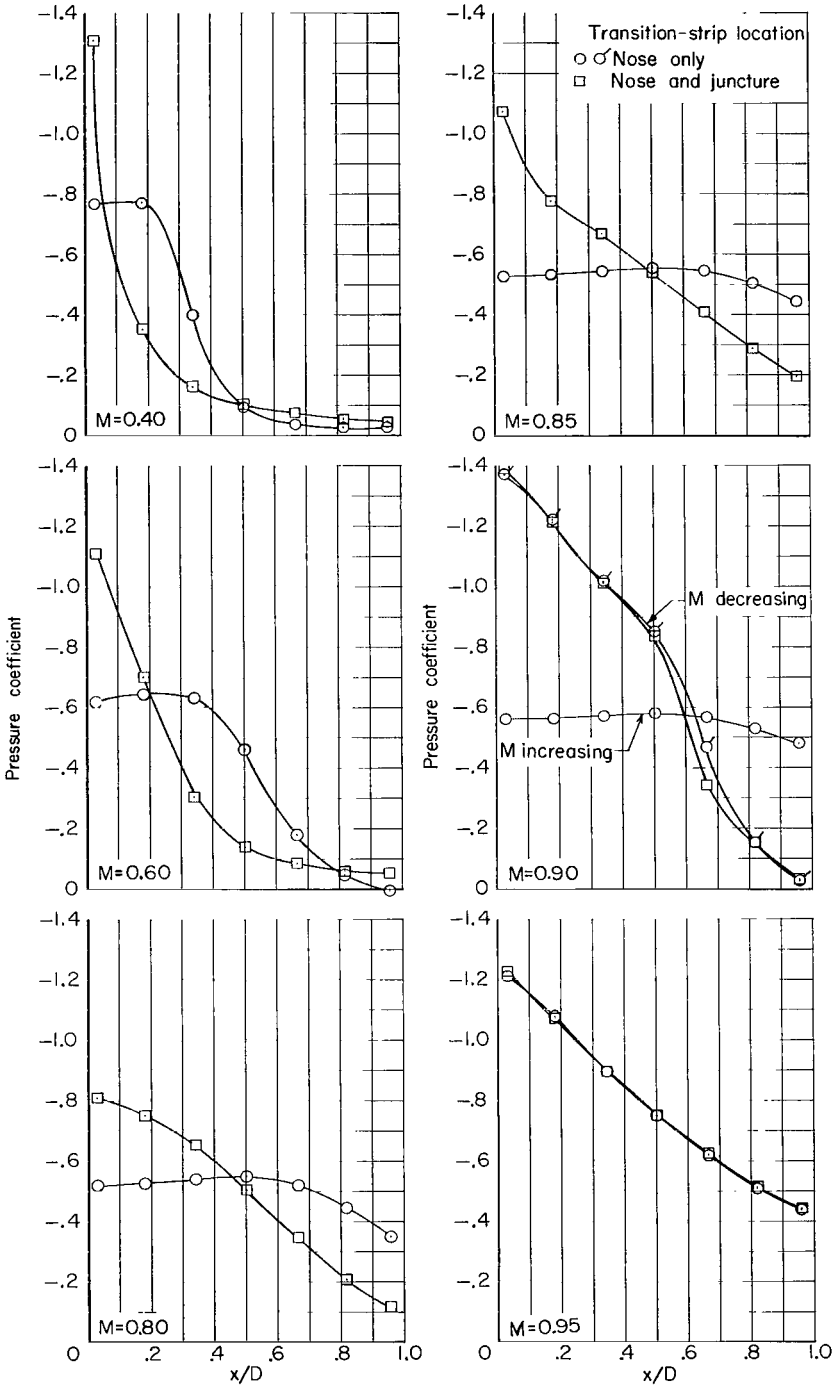

(a) M = 0.40 to M = 0.95.

Figure 5.- Effect of transition-strip arrangement on surface pressure coefficients for cone-cylinder model. $\delta_N = 30^0$; d/D = 1.0; $R_{ft} = 4.0 \times 10^6$.

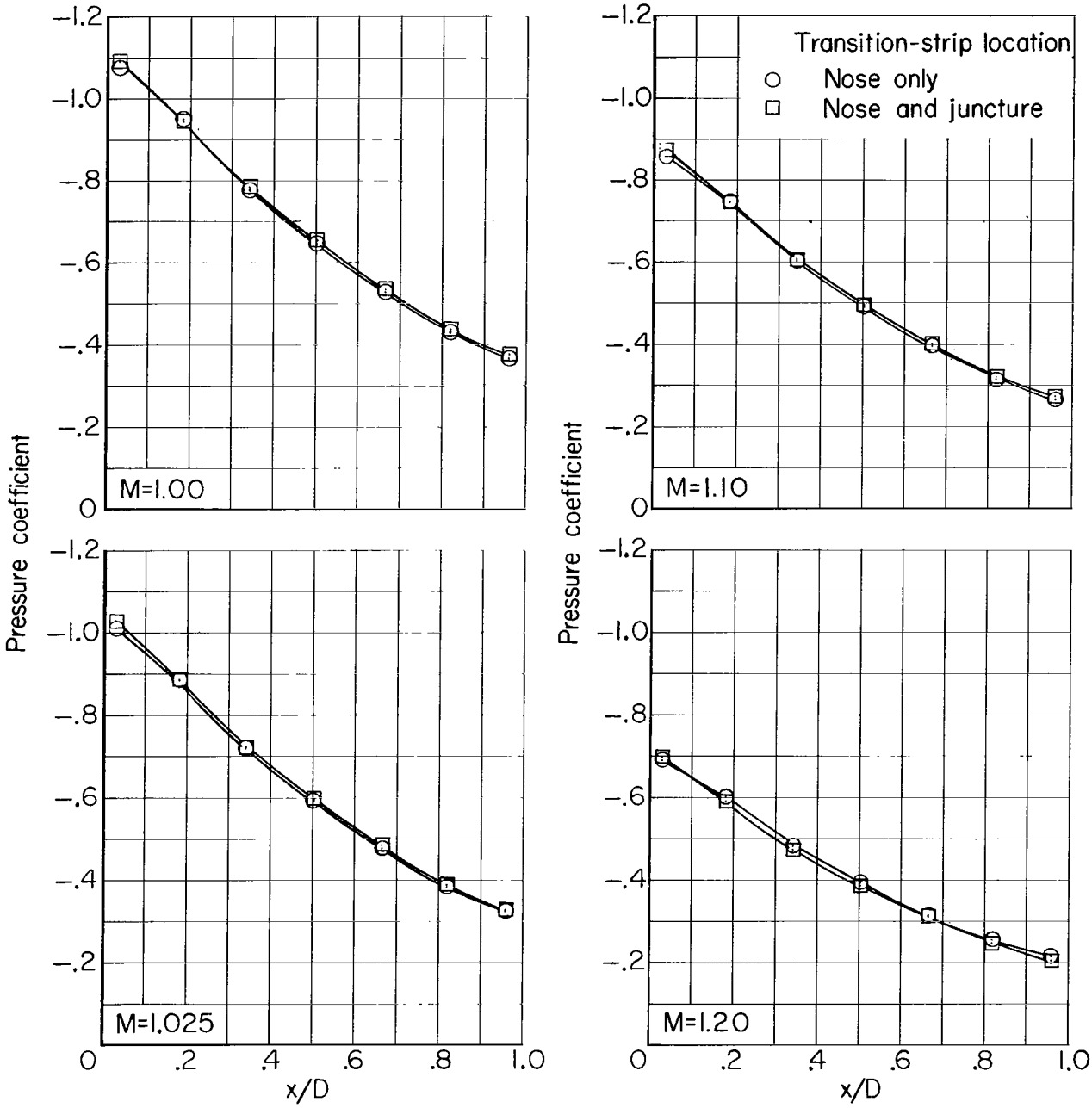

(b) M = 1.00 to M = 1.20.

Figure 5.- Concluded.

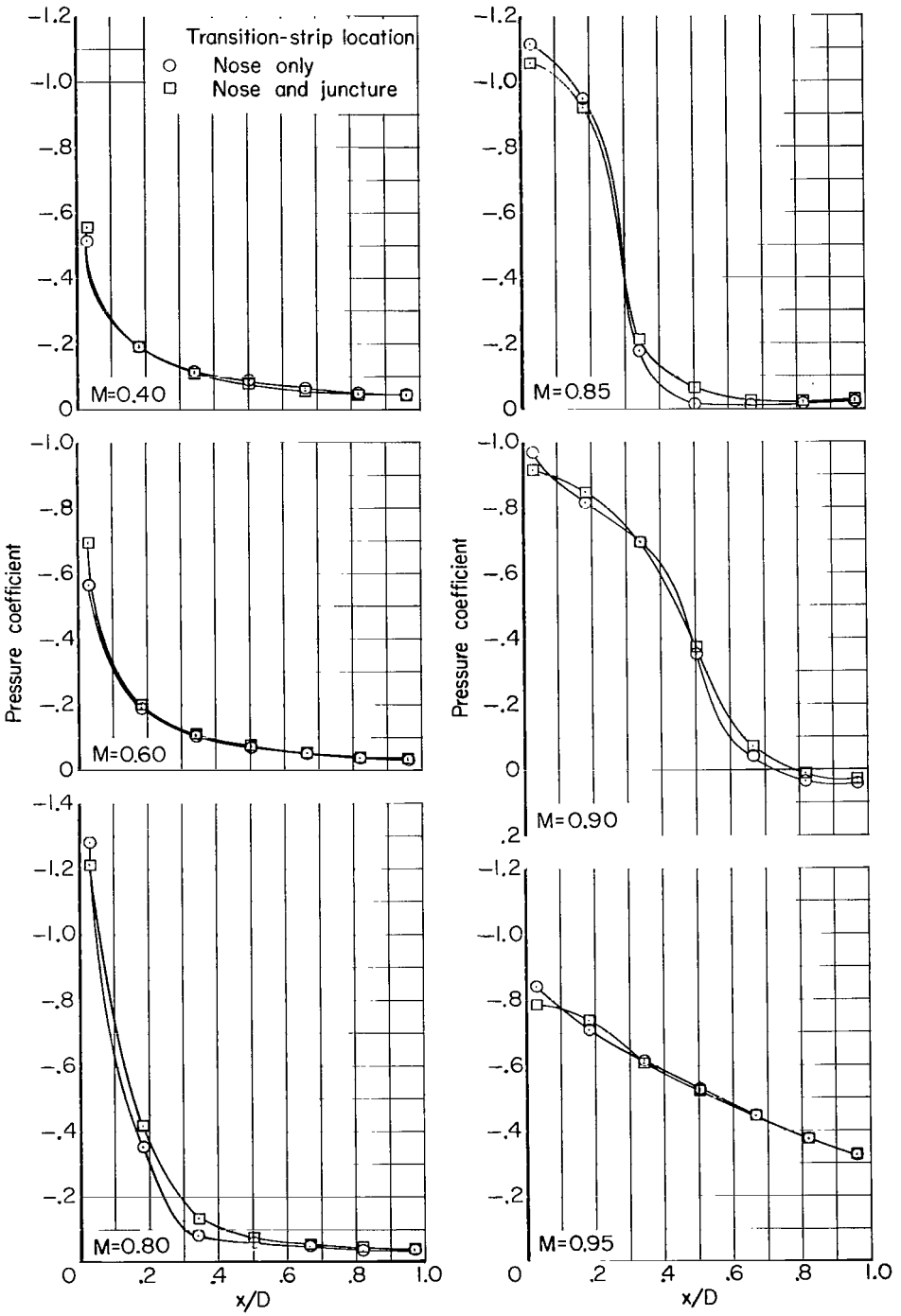

(a) M = 0.40 to M = 0.95.

Figure 6.- Effect of transition-strip arrangement on surface pressure coefficients for cone-cylinder model. $\delta_N = 15^0$; d/D = 1.0; $R_{ft} = 4.0 \times 10^6$.

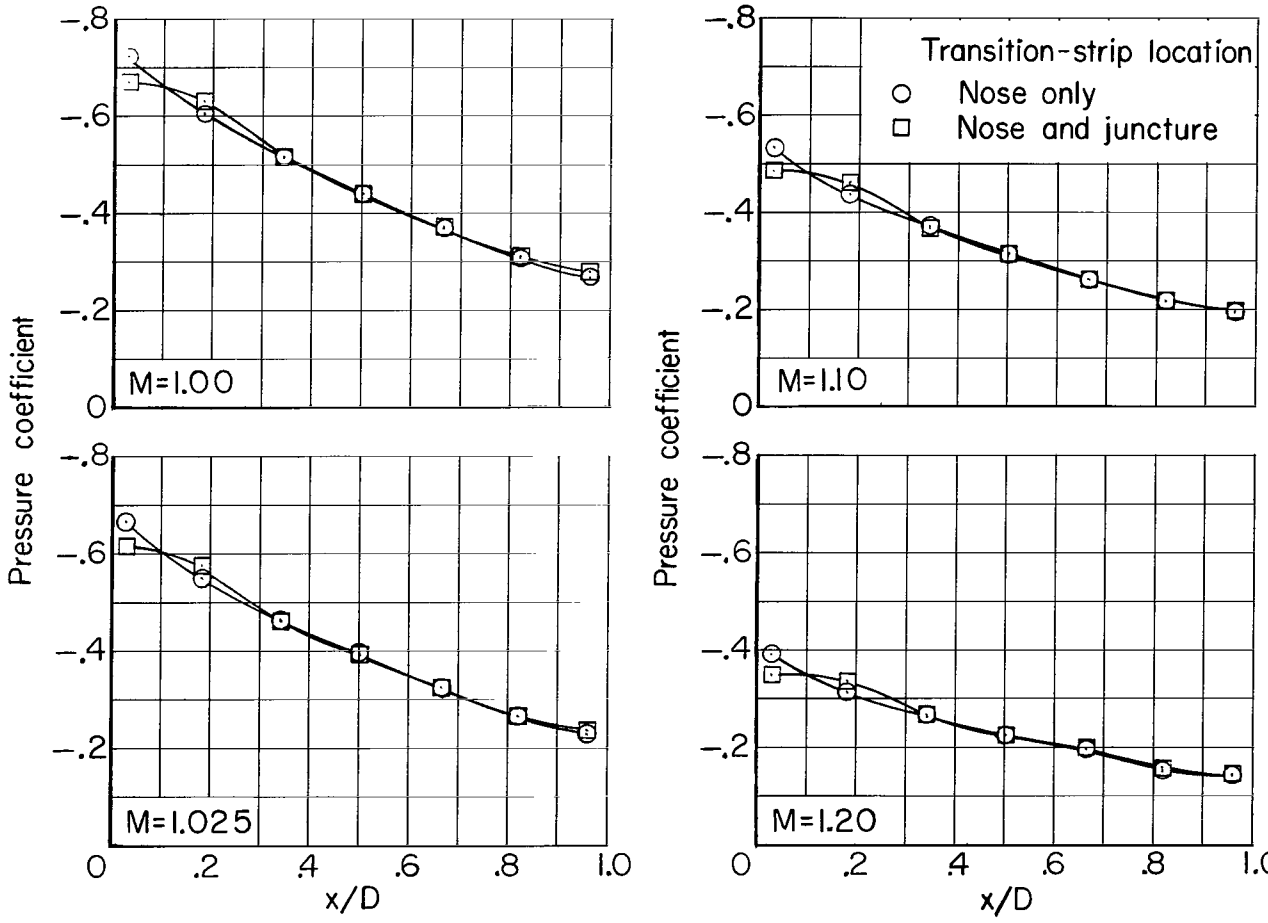

(b) M = 1.00 to M = 1.20.

Figure 6.- Concluded.

Configuration 112; d/D = 0.832

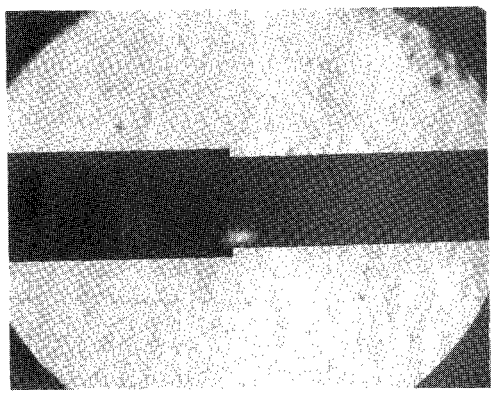

M = 0.80

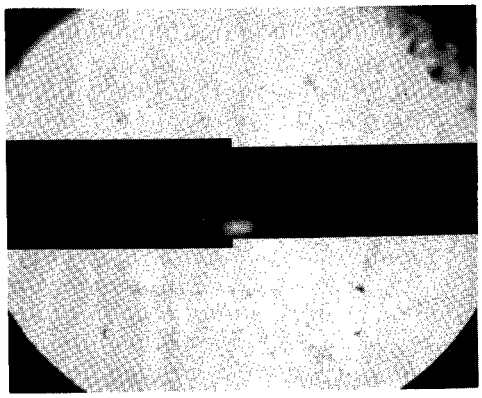

M = 0.90

Configuration 114; d/D = 0.952

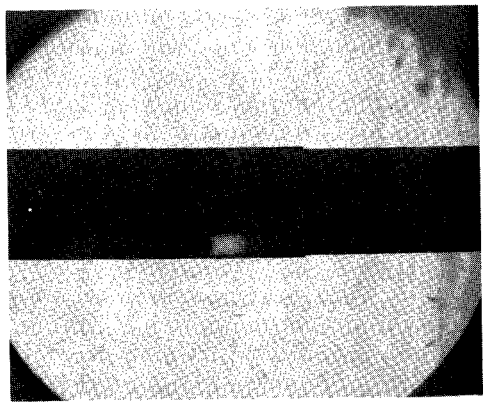

M = 0.90

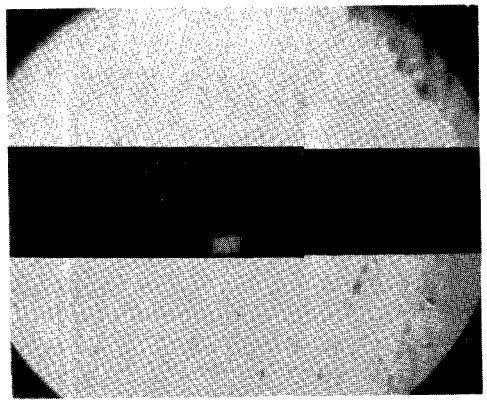

M = 0.95

(a) Configurations 112 and 114; M = 0.80 to 0.95. L-65-90

Figure 7.- Schlieren photographs.

Configuration 134 ; $\delta_N = 15°, l/D = 0.5, d/D = 0.952$

M=1.00 M=1.025 M=1.10 M=1.20

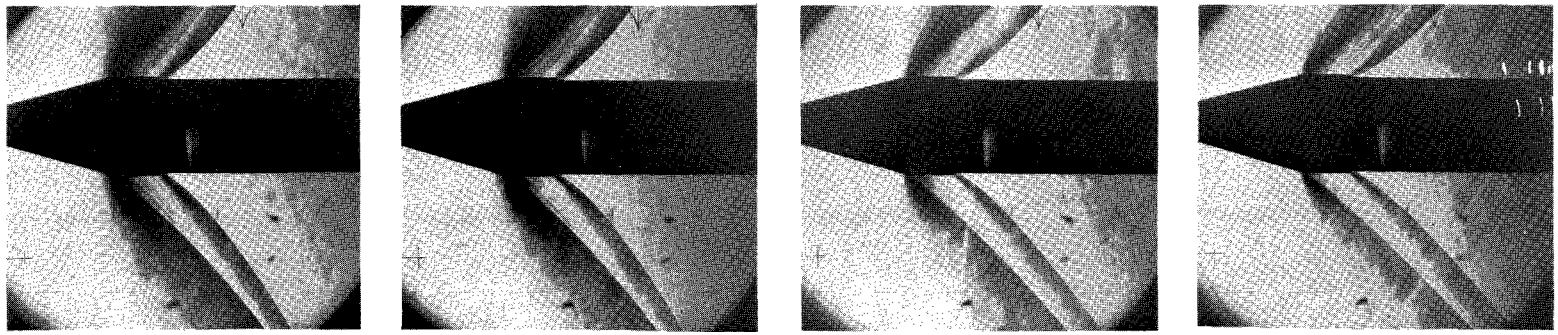

Configuration 234 ; $\delta_N = 30°, l/D = 0.5, d/D = 0.952$

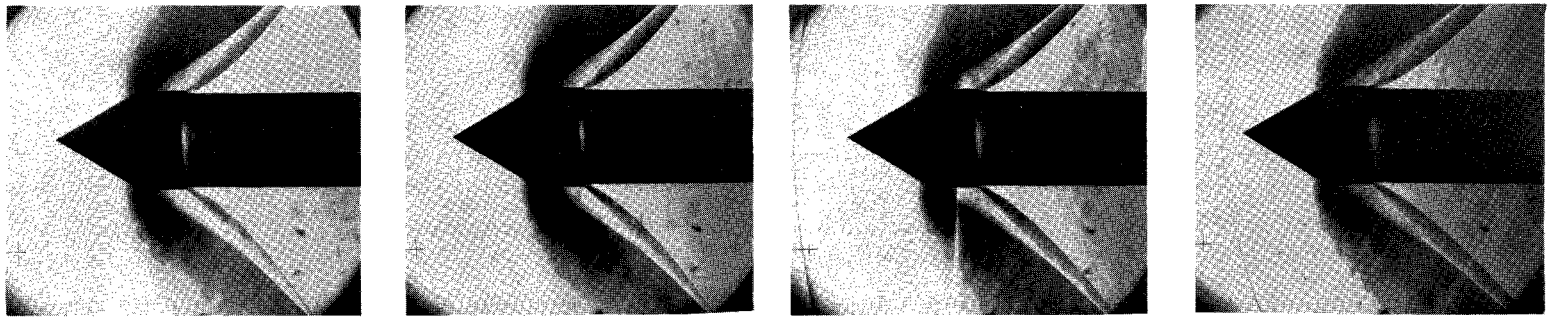

(d) Configurations 134 and 234; M = 1.00 to 1.20.

L-65-93

Figure 7.- Continued.

Configuration 123 ; $\delta_N = 15°$, $l/D = 1.0$, $d/D = 0.910$

M=0.85 M=0.90 M=0.95 M=1.00

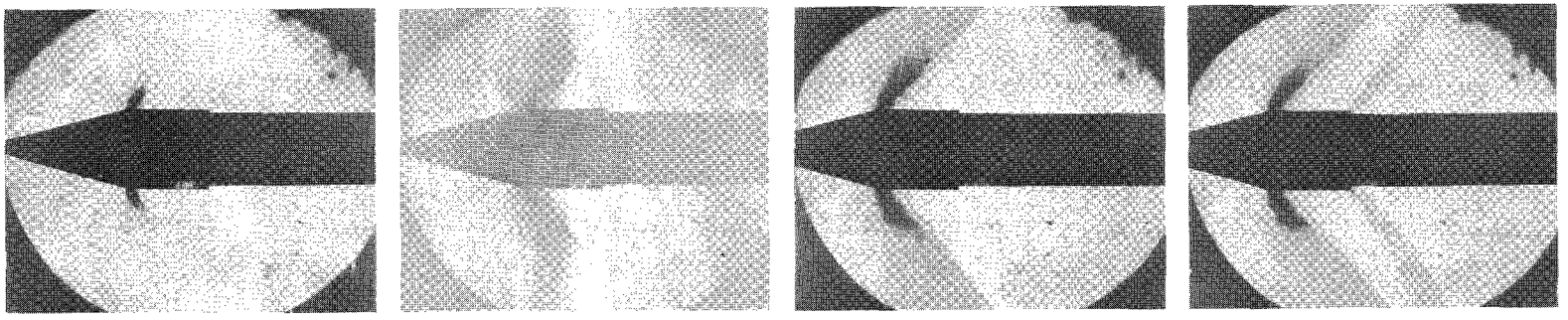

M=1.025 M=1.10 M=1.20

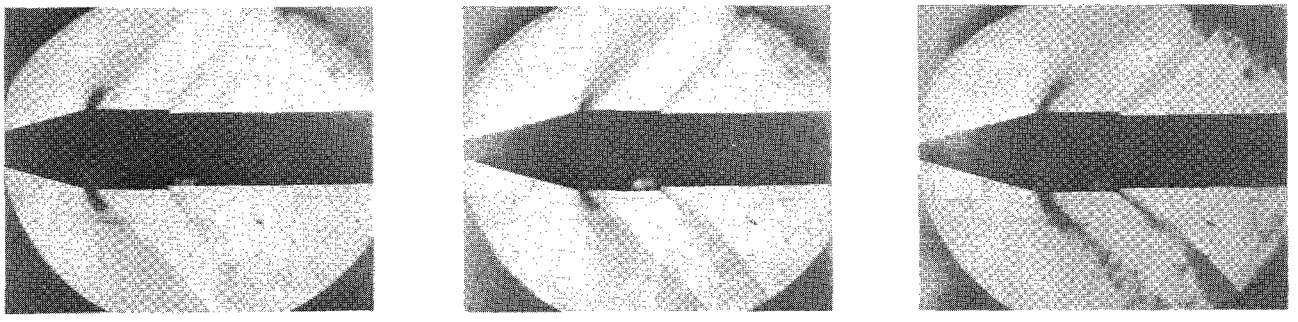

(e) Configuration 123; M = 0.85 to 1.20. L-65-94

Figure 7.- Continued.

Configuration 224 ; $\delta_N = 30°$, $l/D = 1.0$, $d/D = 0.952$

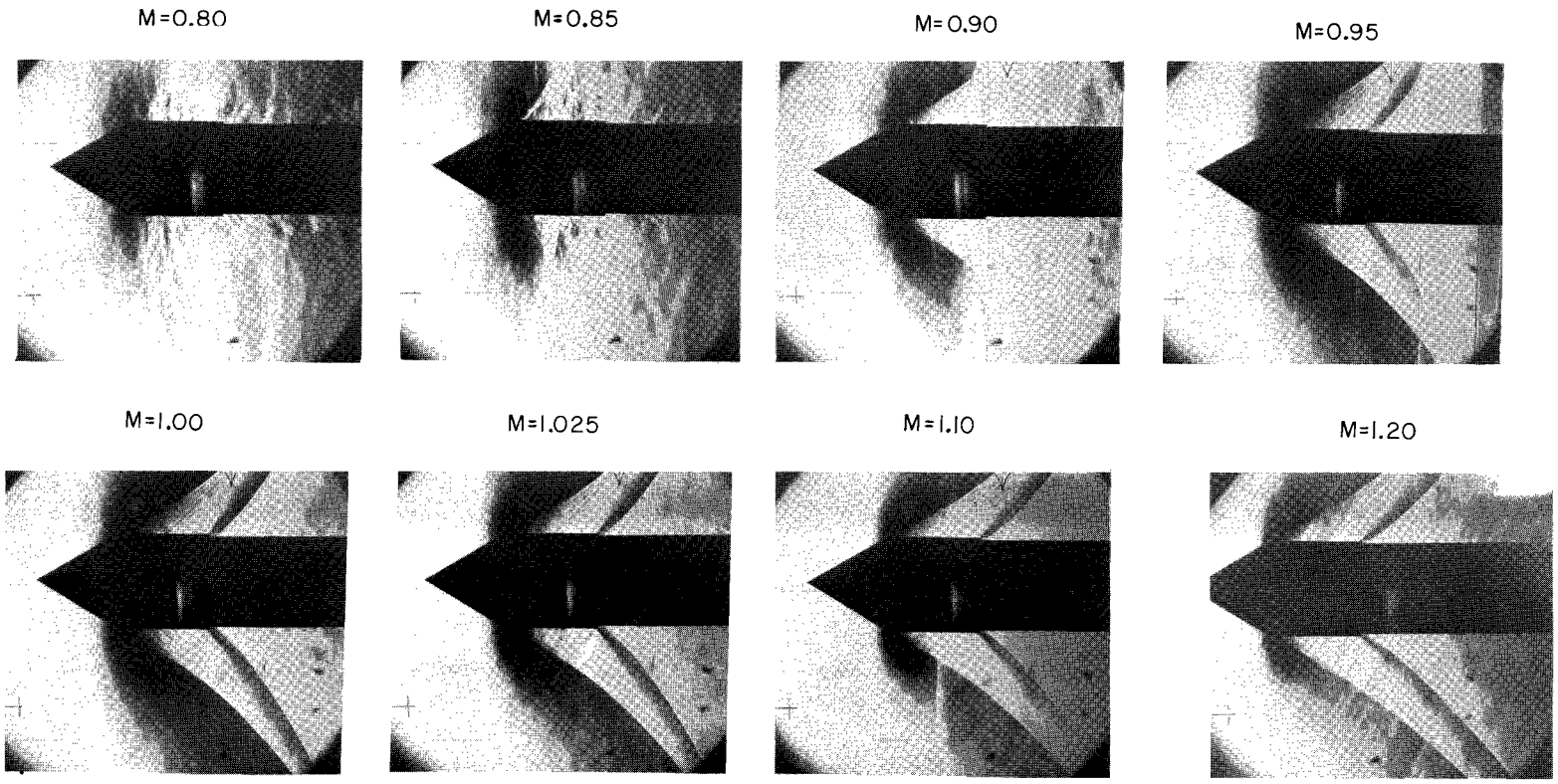

(f) Configuration 224; M = 0.80 to 1.20.

L-65-95

Figure 7.- Concluded.

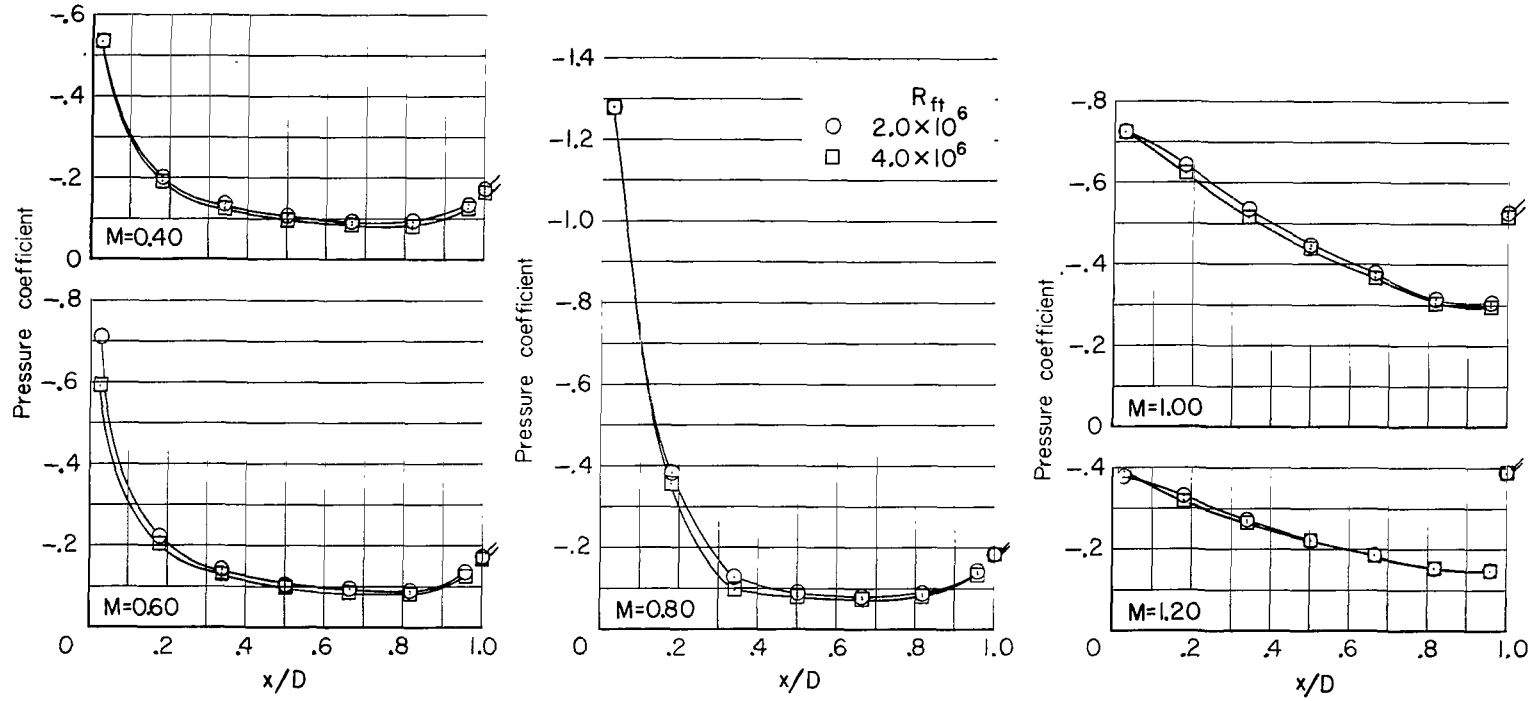

Figure 8.- Effect of Reynolds number on surface and average step base pressure coefficients for cone-cylinder model. $\delta_N = 15^0$; d/D = 0.952; ℓ/D = 1.0. Flagged symbols represent average step base pressure coefficients.

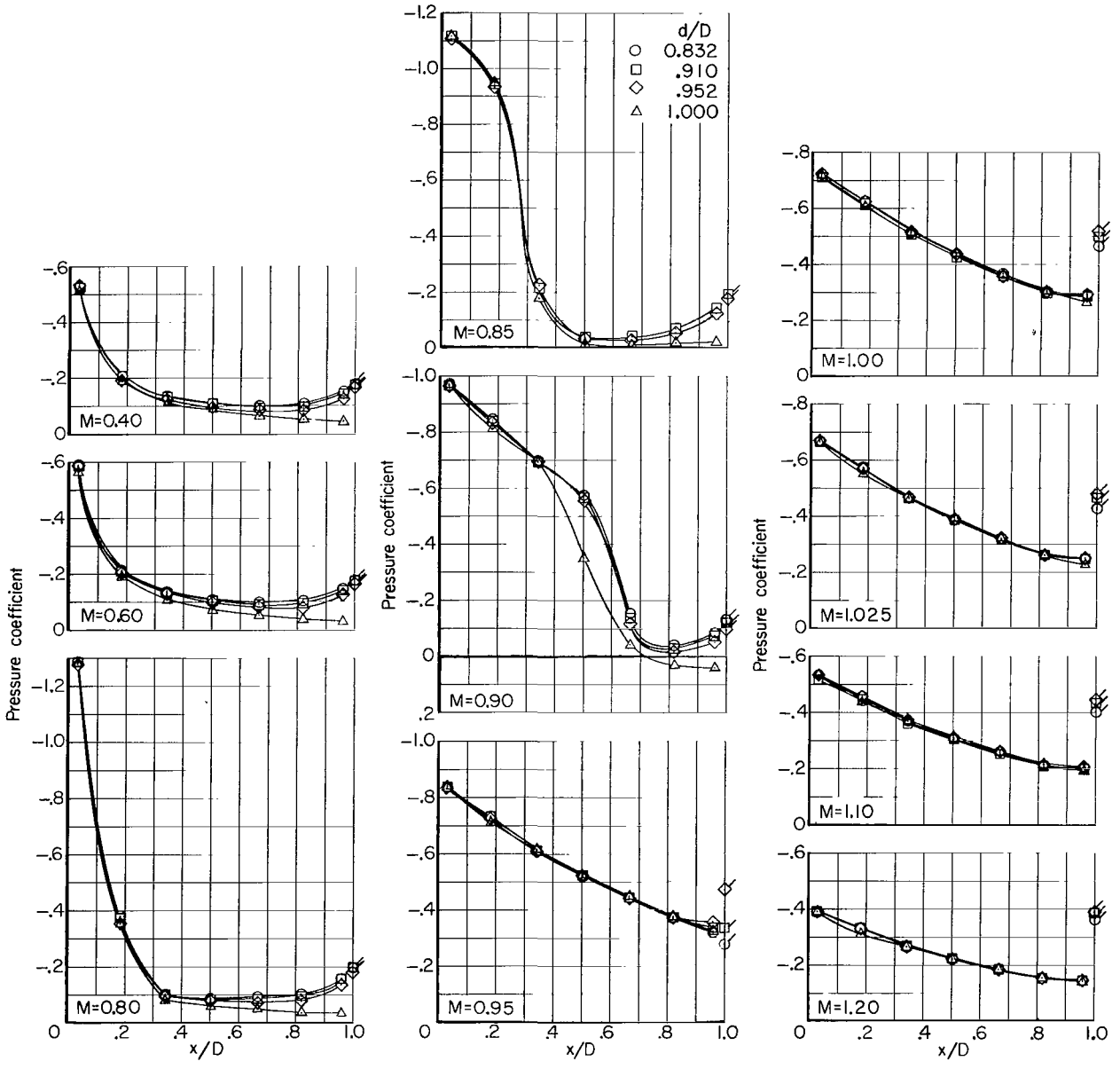

Figure 9.- Effect of step height on surface and average step base pressure coefficients for cone-cylinder model. $\delta_N = 15^0$; $l/D = 1.0$; $R_{ft} = 4.0 \times 10^6$. Flagged symbols represent average step base pressure coefficients.

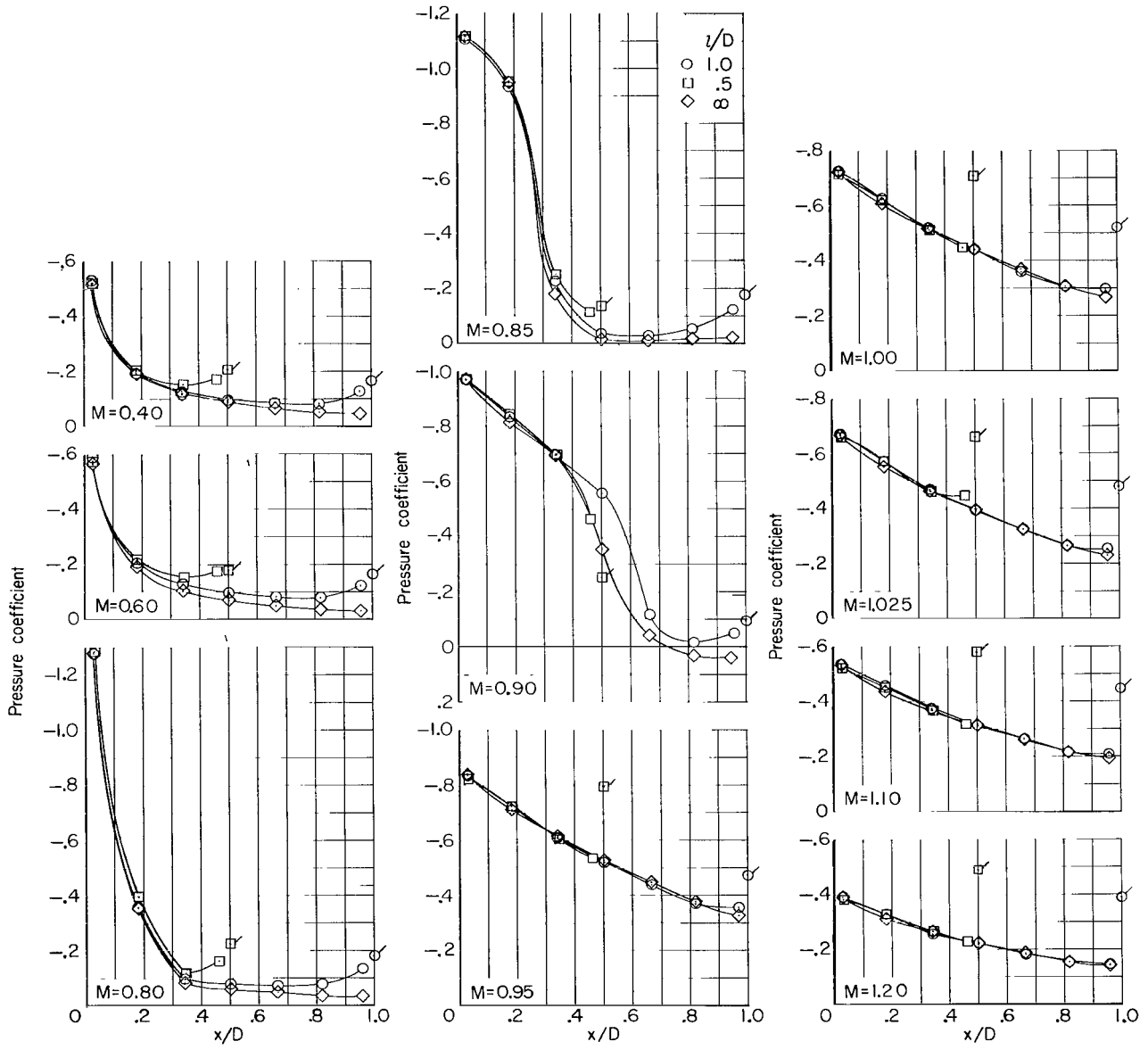

(a) $\delta_N = 15^0$.

Figure 10.- Effect of step location on surface and average step base pressure coefficients for cone-cylinder model. d/D = 0.952; $R_{ft} = 4.0 \times 10^6$. Flagged symbols represent average step base pressure coefficients.

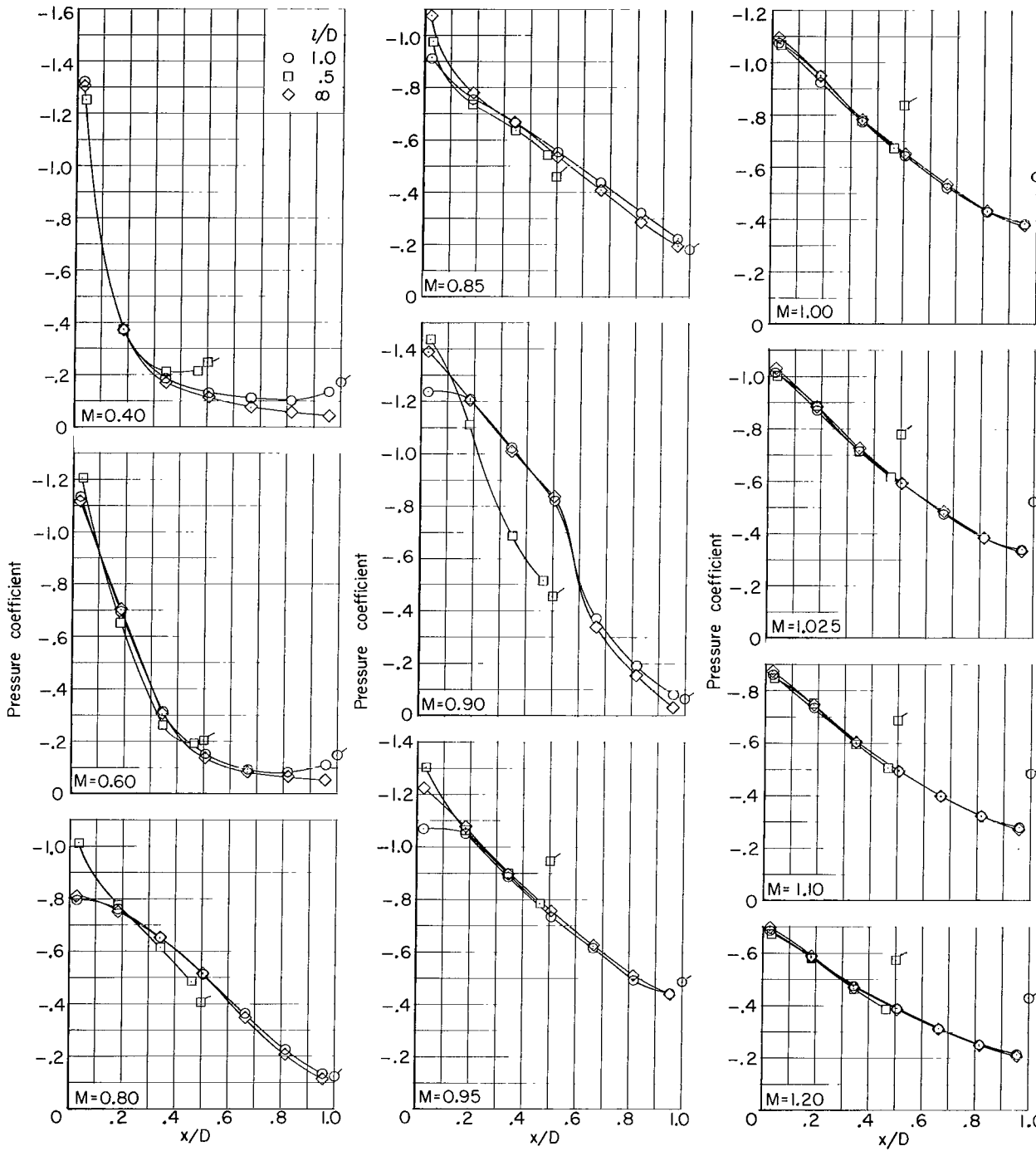

(b) $\delta_N = 30^0$.

Figure 10.- Concluded.

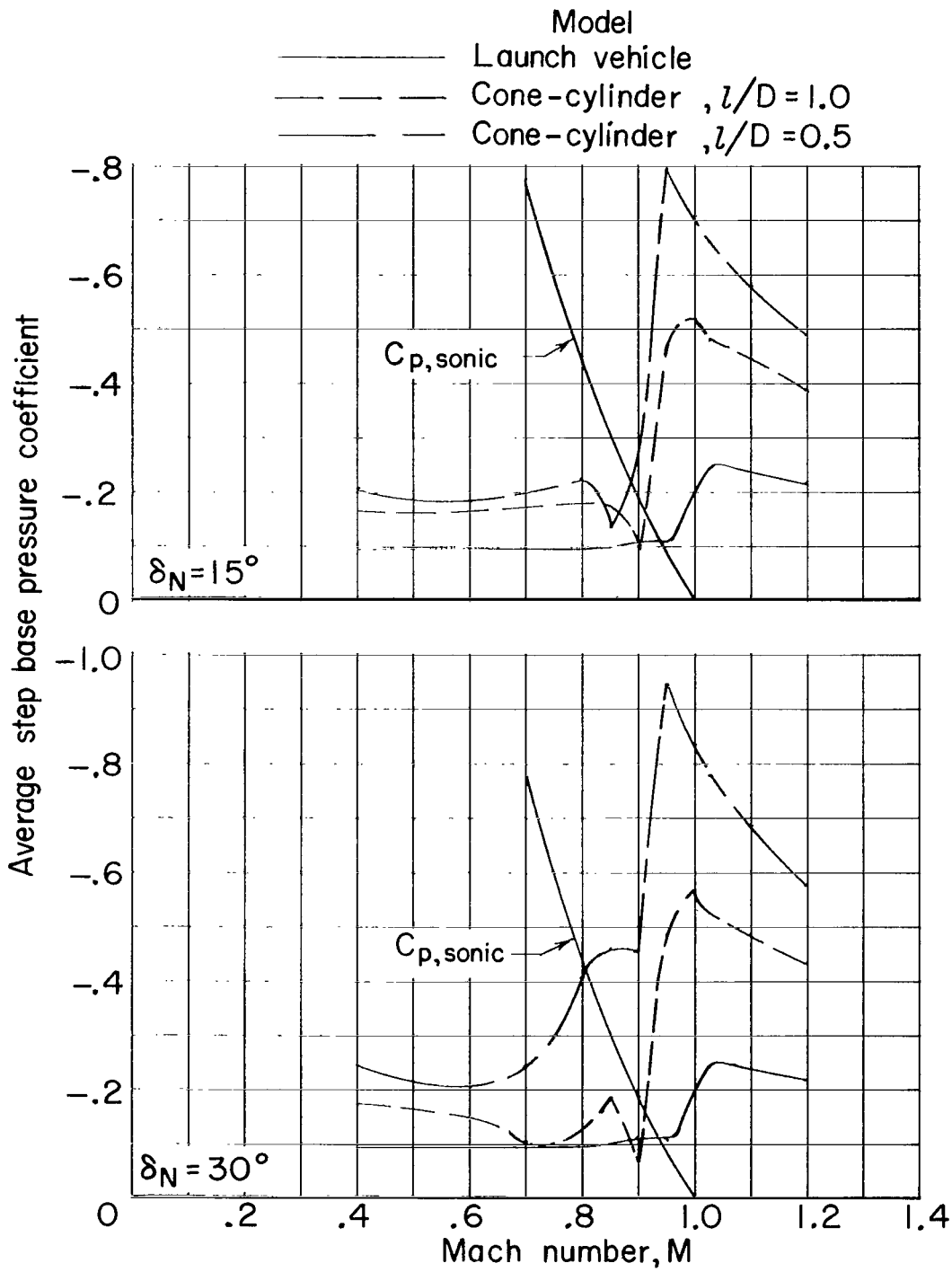

Figure II.- Variation with Mach number of average step base pressure coefficients for several configurations. d/D = 0.952; $R_{ft} = 4.0 \times 10^6$.

2/22/85

"The aeronautical and space activities of the United States shall be conducted so as to contribute . . . to the expansion of human knowledge of phenomena in the atmosphere and space. The Administration shall provide for the widest practicable and appropriate dissemination of information concerning its activities and the results thereof."

—NATIONAL AERONAUTICS AND SPACE ACT OF 1958

NASA SCIENTIFIC AND TECHNICAL PUBLICATIONS

TECHNICAL REPORTS: Scientific and technical information considered important, complete, and a lasting contribution to existing knowledge.

TECHNICAL NOTES: Information less broad in scope but nevertheless of importance as a contribution to existing knowledge.

TECHNICAL MEMORANDUMS: Information receiving limited distribution because of preliminary data, security classification, or other reasons.

CONTRACTOR REPORTS: Technical information generated in connection with a NASA contract or grant and released under NASA auspices.

TECHNICAL TRANSLATIONS: Information published in a foreign language considered to merit NASA distribution in English.

TECHNICAL REPRINTS: Information derived from NASA activities and initially published in the form of journal articles.

SPECIAL PUBLICATIONS: Information derived from or of value to NASA activities but not necessarily reporting the results of individual NASA-programmed scientific efforts. Publications include conference proceedings, monographs, data compilations, handbooks, sourcebooks, and special bibliographies.

Details on the availability of these publications may be obtained from:

SCIENTIFIC AND TECHNICAL INFORMATION DIVISION

NATIONAL AERONAUTICS AND SPACE ADMINISTRATION

Washington, D.C. 20546